A MEDIAL AXIS TRANSFORMATION BASED PROCESS PLANNING METHOD FOR RAPID TOOLING

by

Ziyang He

A thesis submitted to the graduate faculty

in partial fulfillment of the requirements for the degree of

MASTER OF SCIENCE

Major: Industrial Engineering

Program of Study Committee:

Prof. Matthew Frank (Major Professor)
Prof. Frank Peters
Prof. Gap-Yong Kim

The student author and the program of study committee are solely responsible for the content of this thesis. The Graduate College will ensure this dissertation is globally accessible and will not permit alterations after a degree is conferred.

Iowa State University

Ames, Iowa

2017

TABLE OF CONTENTS

Page

ABSTRACT..... iii

CHAPTER 1 INTRODUCTION 4
Overview 4
Motivation 5
Objectives 6
Thesis Organization 7
Reference 7

CHAPTER 2 LITERATURE REVIEW 9
Rapid Prototyping and Applications 9
Laminated Tooling..... 14
Friction Stir Welding 20
Reference 22

CHAPTER 3 PRINCIPLE OF MEDIAL AXIS TRANSFORMATION 26
Relationship between the Medial Axis and the Boundary Curve 26
Bifurcation and Endpoint Processing..... 36
The Exact Solution for Medial Axis Transformation 39
The Equidistant Operation 45
Reference 49

CHAPTER 4 A MEDIAL AXIS TRANSFORMATION BASED PROCESS PLANNING METHOD FOR RAPID LAMINATED TOOLING..... 50
Introduction 51
Methodology 54
Development of overall algorithm towards automated process planning 58
Case Studying 66
Conclusion and future works 70
Reference 71

APPENDIX Medial Axis Transformation Code 72

ABSTRACT

This thesis presents an algorithm to automatically select the positions for friction stir spot welding (FSSW) in a laminated rapid tooling process. The work combines a two-dimensional structural analysis with tool path planning to realize the overall process planning for the rapid tooling of a plastic injection mold. The work starts from a two-dimensional cantilever beam model, defining the effective distance of a single spot joint strength, and also considers the effect of a single layer thickness. Secondly, an efficient medial axis transformation algorithm, which is suitable for the general two-dimensional boundary curves, has been proposed to generate the adaptive equidistance offsetting curves. In addition, through different working conditions of the internal and external spot welds, an adaptive discretization method is presented. Then, a selection principle for choosing the initial spot weld location and processing order with optimization to avoid redundancy is presented. Finally, the authors compare the advantages of this novel algorithm and traditional path planning algorithms with respect to strength and processing efficiency while taking into account structural strength.

CHAPTER I

INTRODUCTION

1.1 Overview

Additive Manufacturing (AM) provides a significant increase in speed and reduction in cost, especially for small production runs and complex geometry products. Although its original motivation was for prototyping, today Additive Manufacturing (AM) is considered a viable production manufacturing method [1] and many Rapid Manufacturing (RM) techniques can produce parts with excellent quality [2]. Currently, companies are experiencing increasing pressure to produce complex and diverse products in shorter product development cycles, aiming to achieve lower overall cost with improved quality [3]. Whereas many methods are for direct manufacturing of parts, rapid tooling is the processing of a mold, pattern or die directly from a CAD model in and additive manner. Laminated tooling is one of the efficient methods for producing metallic molds sufficient strength in that short period of time.

Despite the inherent advantages in the laminated tooling technology, there are two major concerns; layer integrity and automated process planning. Layer deflection in metal laminated tooling is can be the result of insufficient bonding and can arise during post-machining. Since the body of the tooling is separated into various layers, there is always a need to use connections such as bolts, pins, and in the past electric welding processes. Unfortunately, all these methods will have influence on deflection and even may cause plastic deformation on some metallic materials. The other problem is how to achieve automatic process planning with combining post

CNC machining, or an integrated CNC machine and software. Although structural performance evaluation of laminated tooling has been discussed since the 1970s, researchers are focused on finite element analysis and modular analysis validation in a post-manufacturing analysis. The issue is that one also needs to consider "within" process issues during the layer based creation of the tooling. This requires an iterative design, where we need to input slice geometry during the process planning stage. However, current commercial finite element analysis (FEA) and modular analysis packages are very computational expensive. In view of this, some researchers are using computer graphics based algorithms to show geometric weakness areas, and have successfully realized iterative design methods [4]. The limitation is that for engineering applications, a pure geometry analysis is not sufficient to analyze strength requirements. This thesis will mainly focus on taking into consideration strength requirements in the development of an automatic process planning method for layer based rapid tooling process.

1.2 Motivation

Although the traditional adhesive bonding between layers is simple and adaptable, the strength of an adhesive bond will not be sufficient for a metallic injection mold tool. Therefore, this work is focused on a friction stir spot welding (FSSW) based bonding technique, which is proposed to have sufficient strength and strong resistance to inter-layer shear force. The problem is to determine the number and location of spot welds sufficient to bond layers together. Since the friction welding process can be time consuming, we additionally desire a minimal number of such welds. As such, we need to determine the maximum spacing allowable between neighboring spots. In this work a structural model using theoretical analysis of shear forces,

tensile forces and ramp buckling forces coming from both manufacturing and working conditions will be used to determine the spacing Additionally, due to different working conditions, at internal and boundary points are treated separately. Furthermore, algorithms will output specific optimized welding patterns for every layer automatically based on offsetting distance, material properties, predetermined layer thickness, and redundancy optimization. This overall goal is to make friction stir welded tooling a cost effective and capable approach to rapid manufacturing.

1.3 Objectives

The objectives of this thesis are:

1. **Use structural modeling to determine physical process parameters**

Considering material properties, manufacturing and working conditions of the FSSW-based rapid tooling process, structural modeling will be used to generate the effective distance for spacing welds. This will become a physical combining point for geometric process planning.

2. **Develop an efficient medial axis transformation method specific for rapid laminated tooling**

Traditional medial axis transformation methods are either lacking accuracy or cannot be used for the general complex planar domain. In the nature of finding the minimum thickness and skeleton of two dimensional geometry, this work will use a decomposition strategy to divide

complex geometry into three types of simple polygons. Adaptive offsetting methods will also be introduced to realize the generation of equidistant lines with continuity.

3. **Developing criteria for discretization and weld point location**

When the adaptive equidistant lines are generated, discretization becomes very important since our ultimate goal is to seek an optimal spot welding pattern. A largest diagonal distance algorithm will be used for searching the first spot points, and the distance between vertical point pairs will be compared with effective distance to decide if additional spots are needed.

1.4 Thesis Organization

This thesis is divided into five chapters. The current chapter begins with an overview and motivation of this research. *Chapter 2* contains the a literature review, with focus on friction stir spot welding, rapid prototyping and rapid tooling and existing processing planning methods. *Chapter 3* reviews the existing medial axis transformation methods, and proposes a new method to find some critical feature points, such as three-tangent-point circle. The proposed process planning method is presented in *Chapter 4*.

Reference:

[1] Boonsuk, Wutthigrai, and Matthew C. Frank. "Automated fixture design for a rapid machining process." Rapid Prototyping Journal 15, no. 2 (2009): 111-25. doi:10.1108/13552540910943414.

[2] Wong, Kaufui V., and Aldo Hernandez. "A Review of Additive Manufacturing." ISRN Mechanical Engineering 2012 (2012): 1-10. doi:10.5402/2012/208760.

[3] Chua, Chee Kai., Kah Fai Leong, and Chu Sing Lim. Rapid prototyping: principles and applications. New Jersey: World Scientific, 2010.

[4] Zhou, Qingnan, Julian Panetta, and Denis Zorin. "Worst-case structural analysis." ACM Transactions on Graphics 32, no. 4 (2013): 1. doi:10.1145/2461912.2461967.

CHAPTER 2:

LITERATURE REVIEW

2.1 Rapid Prototyping and Applications

Rapid prototyping (RP) is a group of techniques used to quickly fabricate physical models and parts using three-dimensional computer-aided design (CAD). The part is generated using layer by layer deposition of materials.[1] RP has been developed to reduce the product development time and to reduce the cost of manufacturing. As a result, RP offers the potential to revolutionize the product design and manufacturing industry.

Different types of RP methods have been developed since the 1980s. RP processes can be categorized in terms of the state of materials before forming the parts, such as liquids, powders, or solid sheets, or the way by which layers are created, such as lasers, hot rollers, or binders.

One of the early patents in RP was issued to Charles Hull in 1986 for inventing stereolithography (SLA). SLA is considered the first RP technique worldwide. It is a process to make polymers harden under ultraviolet (UV) light and setting up the apparatus for making an object by layer deposition. The first object that he built was a cup 5cm tall, which took Hull months to fabricate it. Two years later, Hull cofounded 3D Systems Corporation, one of the largest and most prolific organizations operating in the 3D printing sector today.[2]

During this process, curable materials, like UV curable materials, are fabricated layer by layer to form the object. The component is fabricated on a build platform submerged in a UV curable liquid photopolymer vat. The beam of UV light is directed by x and y scanning mirrors to shine on the cross section of liquid, and the liquid exposed to it will be cured to create a layer. Once a layer is complete, the build platform is moved down by the thickness of one layer to make room for creating the next layer. This process is repeated until the final part is formed. The completed part is carefully removed from liquid and separated from the platform. The excess resin is removed by chemical bath, and the part is cured again under UV light.[3]

Fused deposition modeling (FDM) was developed by Scott Crump in the late 1980s, and the first FDM system was launched by Stratasys Inc. in the early 1990s.[4] It is a layer additive manufacturing process that uses thermoplastic materials or metal wires to produce parts. The heated thermoplastic filaments are extruded from the nozzle that moves in the horizontal x-y plane while the build platform moves down in the z axis after one layer is built.[5] FDM gains increasing use because of its safe and convenient fabrication process, low cost of materials, and availability of thermoplastics.

Laminated object manufacturing (LOM) is a rapid prototyping process that layers heat sensitive materials like adhesive coated paper, plastic, or metal laminates, which are successively bonded together by heated roller and cut to shape with a laser cutter. Compared with other RP technologies, LOM has some advantages due to peculiarity of the process,[6] such as producing parts with large dimensions and low internal tensions that prevent distortion, shrinking, and

deformation. LOM also can produce wood-like properties when working with paper, but the part complexity is limited.

Selective laser sintering (SLS), invented in the late 1980s at the The University of Texas at Austin,[7] is an RP process that generates complex 3D parts by fusing successive layers of powder materials using a high power laser. The powders can be sintered directly or indirectly with a mix of a thermoplastic binder, depending on the properties of the powders. A beam deflection system makes the laser beam scan each layer according to the corresponding cross section of the component as calculated from a CAD model.[8] When a layer is completed, the bed containing the powders is lowered by one layer thickness to create the next layer. This process repeated until the part is created.

SLS can be used to process almost any type of material, including metals, thermoplastic polymers and elastomers, provided it is available in the form of powders that tend to fuse when heated. SLS also has the advantage to produce parts with high density. The sintered powders form the part while the unsintered powders remains in place and provide structure support. After the component is built, the unsintered powders will be cleaned away and may be recycled.[9]

Laser engineered net shaping (LENS), developed at Sandia National Laboratories (see Fig. 2.1), consists of a nozzle feeding powders to deposition surface, which creates a converging powder stream. The laser beam focuses on the converging point to melt the targeted surface, and the part is created layer by layer. After solidifying, the new part is created or existing parts are repaired.

The deposits were carried out under argon atmosphere. The motion control of the deposit could be from the CAD file or programmed manually.

The LENS method can process more complex geometries due to the 3- or 5-axis systems flexible for the nozzle moves. Parts achieved with LENS usually have a net shape geometry but with a rough finishing. It is necessary to post-process thermally to relieve the internal stress and mechanically to get the desired resolution.[10]

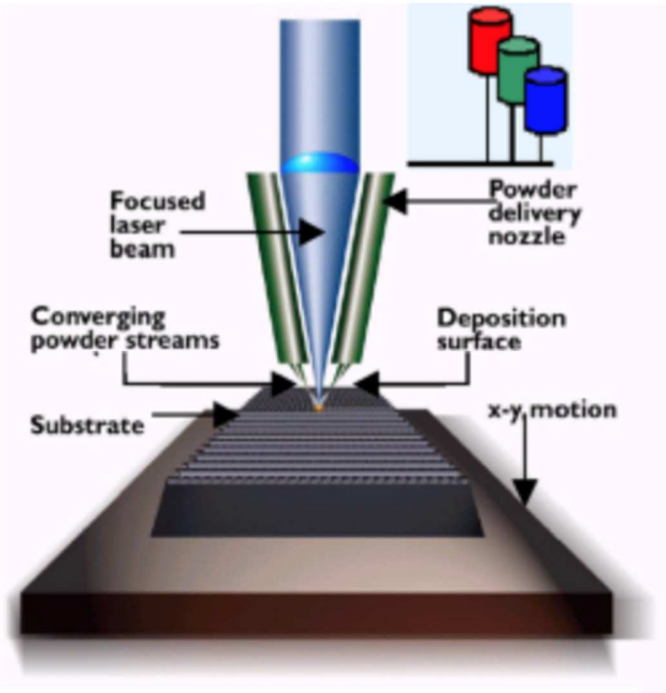

Fig. 2.1 The LENS process (courtesy of Welding Journal)

Three-dimensional printing (3DP), also called binder jetting, is a powder-based rapid prototype technology developed by the Massachusetts Institute of Technology in the 1990s.[11] In this process, each layer starts with a thin distribution of powder spread over the surface of a powder bed. The process is similar to SLS, but instead of using a laser to sinter materials, an ink-jet head

deposits a liquid that selectively joins particles to fuse the powders together. After one layer is formed, the piston that supports the powder bed moves down one layer so the next powder layer can be spread and fused.

The 3DP system has high building speeds and is easy to handle. For metals, 3DP is essentially a powder metallurgy process, so porosity is a major problem. Sometimes infiltration is needed to decrease porosity. Infiltration refers to use a second metal, which is a lower melting temperature alloy to printed structure to achieve dense materials.

RP systems are effective in reducing the time and cost of fabricating new products; however, part accuracy, surface finish, and variety of materials in most RP systems requires improvement. A new form of hybrid RP systems, combining material deposition (RP) and computer numerical control (CNC) machining in a single station, was put forward to find the solution to those problems.[12]

Shape deposition manufacturing (SDM) is a hybrid process that involves depositing materials in a near-net shape on a substrate and then removing unwanted materials using CNC machining (see Fig. 2.2). This process uses microcasting, a weld-based process, to deposit the materials. The part is then transferred to the shaping station for machining, where the desired accuracy and finish are achieved. Stress relief could be used to control residual stress. The robotized pallet system is used to transfer parts between stations. The support material is embedded or deposited and shaped.[13] Varying different materials in the deposition process can change the material properties.

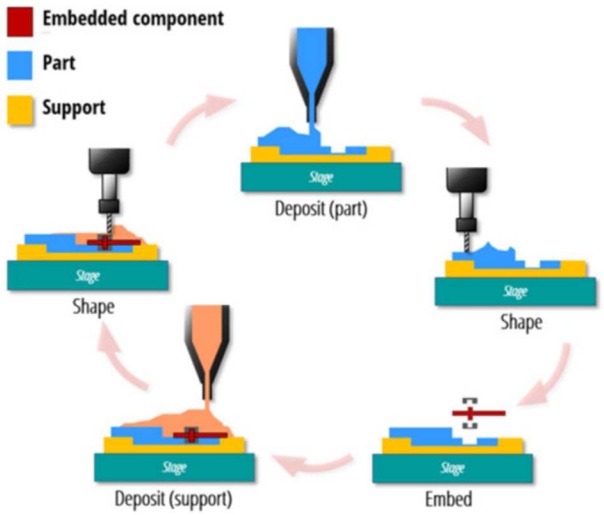

Fig. 2.2 The SDM process cycle with additive and subtractive processes[14]

Solvent welding freeform fabrication technique (SWIFT) is a hybrid RP process based on solvent welding and CNC contour machining.[15] This process is applicable for thermoplastic materials such as polystyrene, which is solvent weldable and available in sheet form. For each layer, a laser printer prints a thin film of high-density polyethylene (HDPE), which is a thermoplastic material not soluble to acetone and therefore serves as a solvent mask. After masking, acetone solvent is applied to the bottom side of the sheet and pressed to the existing stack of sheets where solvent welding take place. Acetone breaks the van der Waal's bonds between polymer chains and thus dissolves the surface of the thermoplastic sheet. The dissolved interfaces of each sheet blend together and form new polymer chains between sheets.

Computer-aided manufacture (CAM) of laminated engineering materials (LEMS) is a hybrid freeform fabrication process for fabricating laminated parts from sheet metals. Laser cutting is applied to materials sheet stock to cut slices. The resulting slices are extracted from the stock to

assemble the component by achieving intimate interlayer contact and subsequent sintering processes.[16]

The main purpose of hybrid processes is to overcome the limitations of RP systems and to improve the quality of the finishes products, especially in surface finish and roughness. The hybrid processes also are expected to improve the cutting rate and materials removal rate, thus reducing the process cost.[14]

2.2 Laminated Tooling

Rapid tooling (RT) refers to a process that uses an RP model to create a mold or uses the RP process to fabricate a tool for a limited volume of prototypes. RT is a natural extension of RP. Compared to conventional tooling, RT provides a significant increase in speed and reduction in cost.

RT is broadly classified as soft tooling and hard tooling and also as indirect tooling and direct tooling. Soft tooling from silicon or epoxy resins or low melting point alloys produces short run and lower volume parts. Hard tooling from materials such as steel and aluminum creates the long run and higher volume of parts. Indirect or pattern-based tooling uses RP-made master patterns to produce molds and dies, while in direct tooling, the layer-by-layer additive process buildup the products. Direct tooling reduces the production time and the inaccuracies introduced by the replication stages.[9]

Rapid laminated tooling is very similar to LOM in many aspects. In the LOM process, sheets of materials are glued together by heated roller and cut to shape with a laser. This process is repeated layer by layer until the part is built, as shown in Fig. 2.3. However, instead of using paper or plastics with adhesive binder, sheets of metals are bolted, bonded with binder, or brazed together in laminated tooling.

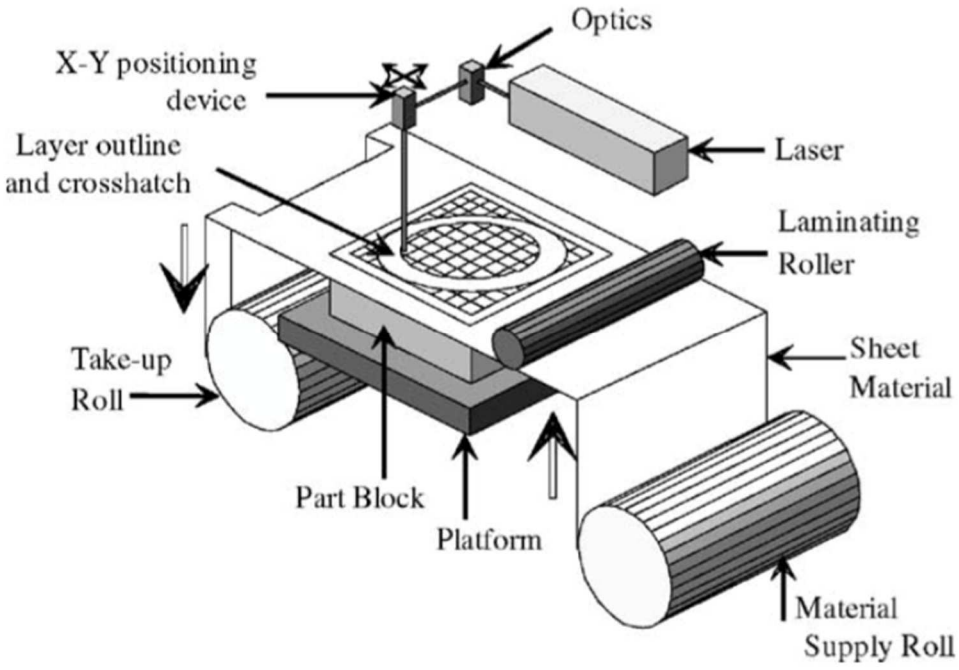

Fig. 2.3 Schematic of LOM processes[17]

Research has been conducted on laminated tooling since the 1980s, when Professor Nakagawa in Japan published the first research in this area.[18] His initial work focused on the manufacture of blanking dies for sheet metal components through a process of stacking horizontal steel sheets. Bainite steel sheets and cheaper steels are used as the tool face and backing plates, respectively. The steel sheets were cut using lasers or a wire EDM process. A test on the qualities of blanked parts and tool life were deemed acceptable.

Soar and Dickens[19] demonstrated a method of laminate tooling for the manufacture of pressure die-casting dies. Due to the high expense of conventional die production, such as die modification after manufacturing, laminated tooling is appealing for the die-casting industry. Aluminum alloy is one of the most applicable casting material for pressure die-casting, while H13 tool steel is considered the only type of steel suitable for aluminum pressure die-casting. Clamping the laser cut H13 steel sheets created the tooling of this process. Although laminated tooling can create low cost, large-scale and flexible dies, there are problems, such as molten materials may force themselves between the laminates and constraints in choosing the thickness of the metal sheets.

Bryden and Pashby[20] used hot platen brazing to join steel sheets together in laminated steel tooling. In this process, the top platen is continuously heated above the liquidus temperature of the braze, such as silver-based alloys or nickel-based alloys. For braze with higher silver content, spraying evenly or selectively on certain areas reduces cost. Nickel-based brazing alloys can be used for higher temperature applications, such as hot creep forming tools. The bottom platen could be heated or cooled to optimize heat flow. The braze is supplied in paste form or evenly sprayed to the lamination. Then, the hot platen brazing is applied to heating and compressing the joints between two platens.

Wimpenny et al.[17] presented Lastform (Large-Scale Tooling for Rapid Manufacture), a three-year research program to develop a method of manufacturing dies for a wide range of aerospace and automotive processes. The research focused on three aspects: laser cutting, cladding and

welding techniques; combined laser sintering and lamination process; and laminate joining methods. The basic manufacturing methodology of laminated tooling is laminate cutting technique, build strategy, surface finishing methods, and choice of laminate materials. Cooling also is an important factor. The tool insert produced under a spiral cooling channel conforming to the tool surface was compared to that in the conventional drilled cooling system and without any cooling. The result showed that conformal cooled inserts were more efficient. The Lastform program has shown the benefit of laminated tooling not only in reducing cost and production time, but also it has the potential in improving the process efficiency through the use of conformal cooling.

Walczyk and Hardt[21] put forward the profiled edge lamination (PEL) tooling method for constructing thick sheet metal forming dies. In this process, thick laminates are stacked and bonded using cutting processes, such as abrasive waterjet (AWJ) machining, laser machining, or flute edge endmilling provided by a CNC cutting trajectory. A PEL die generally has planar die laminations disposed in a vertical plane and stacked together side-by-side in an array. As shown in Fig. 2.4(a), PEL involves the assembly of an array of laminae in which each has a beveled top edge. The top edges of the die laminations form the top surface of the die when placed together in a vertically stacked array. This assembly is achieved by fixing lamina's bottom edge and one adjacent side edge to a fixture. The beveling of each lamina's top edge is achieved by cutting. The clamped PEL tool is shown in Fig. 2.4 (b).

Compared with other cutting methods, AWJ has advantages of getting lamina with more consistent bevel geometry and surface finish. After cutting, the array of processes lamina is

clamped or bonded by applying adhesives or brazing into a rigid tool. The advantages of a PEL array construction over the contoured lamination are that the latter can slide past the profiled-edge cutting means. Thus, laminations only need to be clamped from the side, while unclamped laminations can be individually recut to a new die shape.

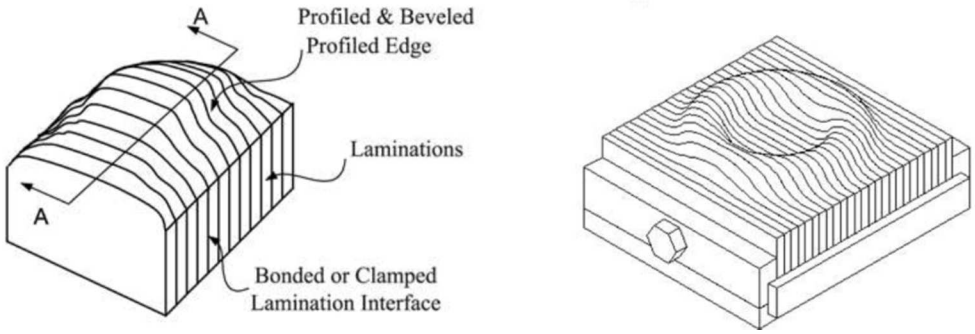

(a) Unclamped PEL tool (b) Clamped PEL tool

Fig. 2.4 Schematics of a PEL tool[22]

Yoo and Walczyk[22] proposed an advanced cutting trajectory in AWJ for PEL. The cutting profiles of PEL are based on intersection curves by slicing the CAD model. The cutting trajectory develops suitable cutting vectors, such as cutting positions and directions that minimize AWJ cutting errors. The PEL's surface quality primarily depends on the AWJ cutting performance. The procedures to generate a suitable AWJ cutting trajectory are creating cutting profiles, stitching profiles together, choosing cutting vectors, and cutting vector compensation. However, this model has its shortcomings. It requires a method to extract exact lamination profiles directly from a CAD model and a cutting trajectory algorithm that improves how the top bevel captures the original CAD geometry and accounts for the limitations associated with AWJ cutting.

Instead of using the build sequence of stack, bond, and cut in commercial LOM process, most laminated tooling processes follow the build sequence of cut, stack, and bond for each layer of materials. The build sequence of stack, bond, and cut has the advantage that accuracy is ensured without aligning each layer precisely. However, it is unfavorable for laminated tooling, because blind laser cutting and the removal of waste materials are difficult for metals. So firstly, the plates are cut into the laminations by laser, or electrical discharge machining (EDM), and the waste materials are removed. Then, the laminations are cleaned and stacked in horizontal or vertical orientation. Finally, the stacked laminations are bonded together.

A variety of bonding methods have been used, such as diffusion bonding, brazing, and bonding with adhesives.[23] Mechanical fasteners also are a commonly used bonding method, using bolts and rivets to join the laminates together. However, a complete automation process is difficult to accomplish using those methods. Among the two building sequences, building laminations by stack, bond, and cut is more amenable for automation.[24]

As a result, a process using a new layer bonding method, a unique combination of industrial adhesives and friction stir welding process of aluminum plates, was proposed.[25] In this process, the adhesives were used to initially secure the aluminum plates for spot welding. Then, the friction stir welding could be continuously applied on the cross section of laminates. After bonding, a three-axis milling machine created accurate 3D shapes and surface finish.

2.3 Friction Stir Welding

Friction stir welding (FSW) is a relatively new solid-state joining process invented at The Welding Institute of UK in 1991. A schematic of FSW is shown in Fig. 2.5. Initially, FSW was applied to aluminum alloys. A non-consumable rotating tool with a specially designed pin and shoulder is inserted into sheets or plates to be joined and traversed along the line of joint. The tool is used to heat up the work piece and move the material to produce the joint. The friction of the tool on the workpiece produces frictional heating, while the rotating pin causes plastic deformation of the workpiece material. The localized heating softens the material around the pin, and the combination of tool rotation and translation leads to movement of material from the front of the pin to the back of the pin where it is forged into a joint.[26]

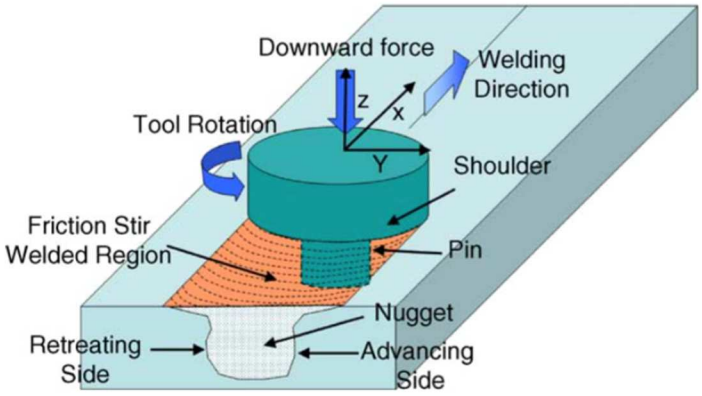

Fig. 2.5 A schematic of Friction Stir Welding[26]

Compared with fusion welding process, any aluminum alloys could be joined with more uniform composition because filler metal is unnecessary in the joining process in FSW. Compared with conventional welding process, FSW is more energy efficient and environment friendly because it uses no gas or flux. However, FSW is a complex process involving material

movement and plastic deformation. Some of the most important factors affecting the FSW process are tool geometry, welding speed, and tool rotational speed.

Tool geometry is critical in FSW process by determining the flow of materials in the welding process. Tool geometry has two primary functions—localized heating and material flow—so the relative size of pin and shoulder are important. The shoulder should be able to provide confinement for the heated volume of materials. Typically, a concaved shoulder and threaded pin are used.

Welding speed and tool rotational speed are important in attaining peak temperature to soften the material. If the rotational speed is not sufficient, then the frictional heat generated is not enough to plasticize the material; the metal in the weld will not diffuse and recrystallize, which will result in holes in the weld. If the rotational speed is too high and the weld speed is too small, then it will generate excessive heat, which will create fluidification cracks in the weld.[27] Thus, finding the proper parameter value for the rotational speed and the weld speed is crucial for a good quality weld.

Reference

1 Thrimurthulu, K., Pandey, P. M. & Reddy, N. V. Optimum part deposition orientation in fused deposition modeling. *International Journal of Machine Tools and Manufacture* **44**, 585-594 (2004).

2 Savini, A. & Savini, G. in *History of High-Technologies and their Socio-Cultural Contexts Conference (HISTELCON), 2015 ICOHTEC/IEEE International.* 1-8 (IEEE).

3 Hull, C. W. (Google Patents, 1986).

4 Masood, S. & Song, W. Development of new metal/polymer materials for rapid tooling using fused deposition modelling. *Materials & Design* **25**, 587-594 (2004).

5 Rayegani, F. & Onwubolu, G. C. Fused deposition modelling (FDM) process parameter prediction and optimization using group method for data handling (GMDH) and differential evolution (DE). *The International Journal of Advanced Manufacturing Technology* **73**, 509-519 (2014).

6 Mueller, B. & Kochan, D. Laminated object manufacturing for rapid tooling and patternmaking in foundry industry. *Computers in Industry* **39**, 47-53 (1999).

7 Kumar, S. Selective laser sintering: a qualitative and objective approach. *Jom* **55**, 43-47 (2003).

8 Yap, C. Y. *et al.* Review of selective laser melting: Materials and applications. *Appl Phys Rev* **2**, 041101 (2015).

9 Pham, D. & Dimov, S. Rapid prototyping and rapid tooling—the key enablers for rapid manufacturing. *Proceedings of the Institution of Mechanical Engineers, Part C: Journal of Mechanical Engineering Science* **217**, 1-23 (2003).

10 Gibson, I., Rosen, D. W. & Stucker, B. *Additive manufacturing technologies*. Vol. 238 (Springer, 2010).

11 Sachs, E., Cima, M., Williams, P., Brancazio, D. & Cornie, J. Three dimensional printing: rapid tooling and prototypes directly from a CAD model. *Journal of Engineering for Industry* **114**, 481-488 (1992).

12 Hur, J., Lee, K. & Kim, J. Hybrid rapid prototyping system using machining and deposition. *Computer-Aided Design* **34**, 741-754 (2002).

13 Merz, R., Prinz, F.B., Ramaswami, K., M., Weiss, L.E. Shape Deposition Manufacturing. *Proceedings of the Solid Freeform Fabrication Symposium* (1994).

14 Chu, W.-S. *et al.* Hybrid manufacturing in micro/nano scale: a review. *International Journal of Precision Engineering and Manufacturing-Green Technology* **1**, 75-92 (2014).

15 Cormier, D. & Taylor, J. A process for solvent welded rapid prototype tooling. *Robotics and Computer-Integrated Manufacturing* **17**, 151-157 (2001).

16 Newman, W. S., Mathewson, B. B., Zheng, Y. & Choi, S. A novel selective-area gripper for layered assembly of laminated objects. *Robotics and computer-integrated manufacturing* **12**, 293-302 (1996).

17 Wimpenny, D. I., Bryden, B. & Pashby, I. R. Rapid laminated tooling. *Journal of materials processing technology* **138**, 214-218 (2003).

18 Nakagawa, T. & Suzuki, K. in *Proceedings of the Twenty-First International Machine Tool Design and Research Conference.* 129-138 (Springer).

19 Soar, R. & Dickens, P. Deflection and the Prevention ofIngress within Laminated Tooling for Pressure Die-Casting. (1997).

20 Bryden, B. & Pashby, I. Hot platen brazing to produce laminated steel tooling. *Journal of Materials Processing Technology* **110**, 206-210 (2001).

21 Walczyk, D. & Hardt, D. in *Proceedings of Solid Freeform Fabrication Conference.* 215-226.

22 Yoo, S. & Walczyk, D. An advanced cutting trajectory algorithm for laminated tooling. *Rapid Prototyping Journal* **11**, 199-213 (2005).

23 Daniel, F. W. & Dolar, N. Y. Bonding Methods for Laminated Tooling.

24 Zak, G. & Wang, W. X. Adhesive Bonding of Sheet for Laminated Metal Tooling. *Proceedings of Solid Freeform Fabrication* (2002).

25 Karthikeyan, R. K. Process planning for rapid manufacturing of plastic injection mold for short run production. (2010).

26 Mishra, R. S. & Ma, Z. Friction stir welding and processing. *Materials Science and Engineering: R: Reports* **50**, 1-78 (2005).

27 Zhi-hong, F., Di-qiu, H. & Hong, W. Friction stir welding of aluminum alloys. *Journal of Wuhan University of Technology-Mater. Sci. Ed.* **19**, 61-64 (2004).

CHAPTER 3:

PRINCIPLE OF MEDIAL AXIS TRANSFORMATION

3.1 Relationship Between the Medial Axis and the Boundary Curve

The medial axis of the planar domain can be seen as the union of all centers of the maximum tangent circles to the boundary curve. The maximum disc is a circle completely contained within the closed curve and at least tangent to the two boundary curves. The medial axis transform (MAT) is the general term for the medial axis of a given domain and its corresponding radius function. In the MAT, these maximum circles are called the medial transformation circle M. We can divide the points on the medial axis into three categories according to the different number of tangent points.

When the medial transformation circle and the boundary curve have two tangent points, the corresponding point on the medial axis is called Normal Point, as shown in Figure 3.1 (a) point N (or in addition to the two ends A, E outside the line, and AE on the point are normal), with point N corresponding to the axis of the circle. The tangent point is shown in Figure 3.1 (b). When the medial transformation circle and the boundary curve have three or more tangent points, the corresponding point on the medial axis is called the Branch Point (Figure 3.1 (a)). Points E and F correspond to the medial transformation circle and tangent point as shown in Figure 3.1(c). When there is only one point on the corresponding axis it is called End Point, as shown in Figure 3.1(a) of the A, B, C, and D points [1] [2].

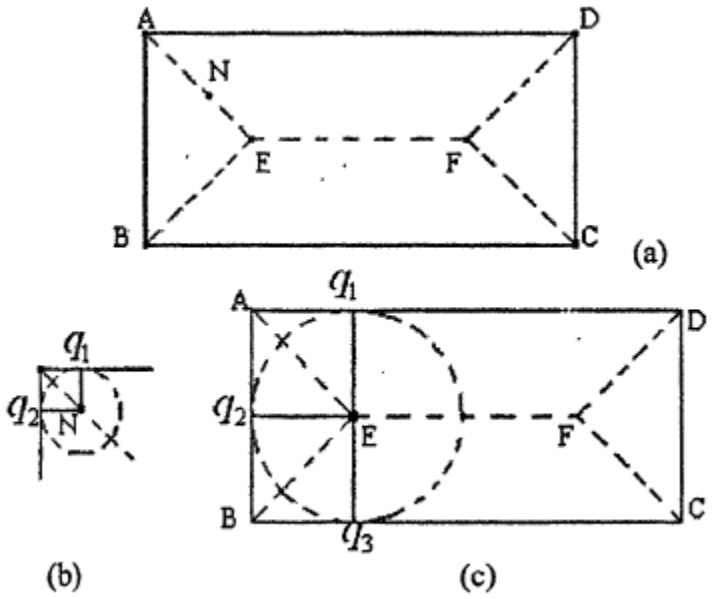

Fig. 3.1 Classification of points on medial axis

3.1.1 Medial axis and rotation line

Assuming there are two free curves on the plane, C_1, C_2, we need to calculate the boundary curve of the medial axis. The union of the center, which is tangent to them and has at least two tangent circles, is the medial axis C. The medial transformation circle has radius r, the corresponding center is point P, and the corresponding two tangent points are called q_1, q_2, as shown in Figure 3.2. According to the characteristics of the plane curve Frenet frame and the concept of accompanying curve, the Frenet frame {p, e_1, e_2}. By using the symmetry of the medial axis, it is reasonable to regard the two boundary curves and the medial axis as two pairs of accompanying curves. Under the condition of the known radial point r (G) of the center point P, S is the natural parameter of the medial axis C, and the vector of the two boundary curves at the tangent points q_1, q_2 can be expressed as:

$$\begin{aligned} r_1 &= r(s) + x_1 e_1 + x_2 e_2 \\ r_2 &= r(s) + x_1 e_1 - x_2 e_2 \end{aligned} \quad (3.1)$$

Where x_1, x_2 are the relative coordinate of tangent point q1 in frame {p, e_1, e_2}.

Taking the differential formula (3.1) on both sides and the use of plane curve Frenet formula, you can get the boundary curve of the tangent vector, with the equation:

$$\begin{aligned} \dot{r}_1 &= (1 + x_1' - kx_2)e_1 + (x_2' + kx_1)e_2 \\ \dot{r}_2 &= (1 + x_1' + kx_2)e_1 + (x_2' - kx_1)e_2 \end{aligned} \quad (3.2)$$

Where k is the curvature of the medial axis C at point P, x_1', and x_2', which are the derivatives of x_1 and x_2, respectively.

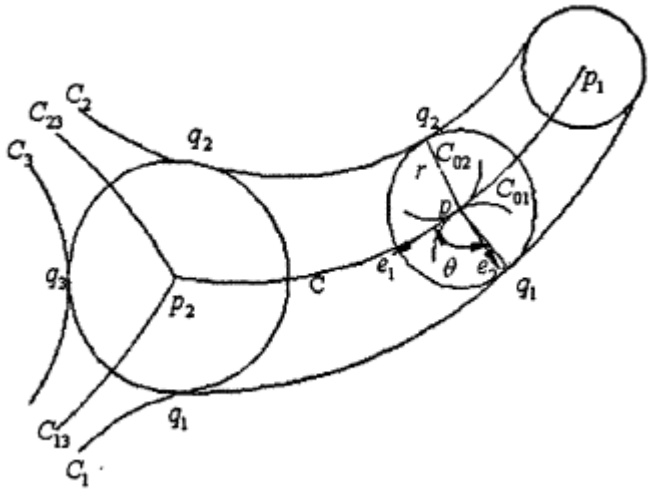

Fig. 3.2 Medial axis and rotation line

As shown in Figure 3.2, if the medial axis C as a static space instantaneous line, C_{01}, C_{02} on the line C do pure rolling with tangent point P, C_{01}, and C_{02} are completely symmetrical with $\mathbf{e_1}$. Assuming that the tangent points q_1 and q_2 are fixed on the C_{01} and C_{02}, the trajectory curves C1 and C2, which are caused by q_1 and q_2 rolled up along the C_{01} and C_{02} in the static space, are called the rotation lines. Because q_1 and q_2 are fixed on C_{01} and C_{02}; curves C, C_{01}, and C_{02} are tangent at point P and have the same Frenet frame. With Cesaro fixed condition, it could be referred to as:

$$\left.\begin{aligned} x_1' &= k_0 x_2 - 1 \\ x_2' &= -k_0 x_1 \end{aligned}\right\} \quad (3.3)$$

Where k_0 is for the curvature of the instantaneous line C_{01}, C_{02} at the P.

Substituting equation (3.3) into equation (3.2) yields:

$$\begin{aligned} \dot{r}_1 &= (k_0 - k) x_2 e_1 - (k_0 - k) x_1 e_2 \\ \dot{r}_2 &= (k_0 + k) x_2 e_1 + (k_0 + k) x_1 e_2 \end{aligned} \quad (3.4)$$

The aforementioned geometric model uses the relative coordinates and the differential invariants k and k_0 to associate the medial axis, the boundary curve with the moving instantaneous line. The boundary curve can be thought of as a rotating line formed by pure rolling on the medial axis C (i.e., the fixed instantaneous line). From the knowledge of differential geometry, it can be seen that the tangent lines of the cyclone lines C_1 and C_2 at q_1 and q_2 must be orthogonal to the vectors $\mathbf{q_1p}$ and $\mathbf{q_2p}$, respectively. So q_1, q_2 in this moment can be seen doing the rotary motion at point P of medial axis to meet the requirements of the medial axis transformation.

Let

$$P_1 = x_1 e_1 + x_2 e_2 \text{、} \quad P_2 = x_1 e_1 - x_2 e_2 \quad (3.5)$$

Now we have:

$$\left.\begin{aligned} \dot{r}_1 \bullet P_1 &= 0 \\ \dot{r}_2 \bullet P_2 &= 0 \end{aligned}\right\} \quad (3.6)$$

Substituting equations (3.2) and (3.5) into equation (3.6), we could have:

$$x_1 + x_1 x_1' + x_2 x_2' = 0 \quad (3.7)$$

Because $r^2 = x_1^2 + x_2^2$, equation (3.7) could be simplified as:

$$r' = -x_1 / r = \cos(\theta) \quad (3.8)$$

Where the θ is the angle between $\mathbf{q_1p}$ and $\mathbf{e_1}$.

For a given boundary curve C_1 (U_1), C_2 (U_2), where U_1 and U_2 are the parameter of the curve, in order to establish the relationship between the point P on the medial axis and the tangent point q_1 and q_2 on the corresponding boundary curve, it is first necessary to determine the parametric relationship between them. Let the vector of the boundary curves C_1 and C_2 be:

$$\begin{aligned} R_1(u_1) &= r_1(s) \\ R_2(u_2) &= r_2(s) \end{aligned} \quad (3.9)$$

We deviate equation (3.9) and substitute equation (3.4) into it:

$$\left.\begin{aligned} \dot{R}_1 d(u_1) &= \dot{r}_1 ds = (k_0 - k) x_2 ds e_1 - (k_0 - k) x_1 ds e_2 \\ \dot{R}_2 d(u_2) &= \dot{r}_2 ds = (k_0 + k) x_2 ds e_1 + (k_0 + k) x_1 ds e_2 \end{aligned}\right\} \quad (3.10)$$

The differential relationship between the boundary curves C_1 and C_2 and the axis C parameter can be solved by equation (3.10):

$$\left.\begin{aligned} \frac{du_1}{ds} &= \frac{(k_0 - k) r}{\left\| \dot{R}_1 \right\|_2} \\ \frac{du_2}{ds} &= \frac{(k_0 + k) r}{\left\| \dot{R}_2 \right\|_2} \end{aligned}\right\} \quad (3.11)$$

Here, $r^2 = x_1^2 + x_2^2$ is the radius of the medial transformation circle. In equation (3.11), the curvature k_0, k_1 becomes the key to solve the problem. Using the Euler–Savary formula, the curvature expression of the boundary curves C_1, C_2 at point q_1 and q_2 can be obtained as follows:

$$\left.\begin{aligned} k_1 &= -\frac{1}{r} + \frac{\sin\theta}{(k_0 - k) r^2} \\ k_2 &= \frac{1}{r} - \frac{\sin\theta}{(k_0 - k) r^2} \end{aligned}\right\} \quad (3.12)$$

Solving the equation (3.12), we could get k_0 and K as follows:

$$k_0 = \frac{\sin\theta\left[2 + r\left(k_1 - k_2\right)\right]}{2r\left(1 + k_1 r\right)\left(1 - k_2 r\right)} \quad (3.13)$$

$$k = \frac{\sin\theta\left(k_1 + k_2\right)}{2\left(1 + k_1 r\right)\left(1 - k_2 r\right)} \quad (3.14)$$

This shows the relationship between the boundary curve and the curvature of the medial axis.

3.1.2 Moving frame for medial axis and boundary curve

The abovementioned method of determining the relationship between the boundary curve and the medial axis is based on the concept of the rotation line, which treats the points on the boundary curve as fixed points on the rotation lines C_{01} and C_{02}, and studies the relationship between parameters and curvature when C_{01} and C_{02} are purely rolling on the central axis C. If we establish the Frenet frame $\{p, \mathbf{e_1 e_2}\}$ of the central axis C at the point P and the Frenet frame $\{q_1, e_1^{(1)} e_2^{(1)}\}$ of the curves C_1 and C_2 are set at q_1 and q_2, respectively, with $\{q_2, e_1^{(2)} e_2^{(2)}\}$, as shown in Figure 3.3. Furthermore, s, s_1, and s_2 are the natural parameters of C, C_1, and C_2, respectively.

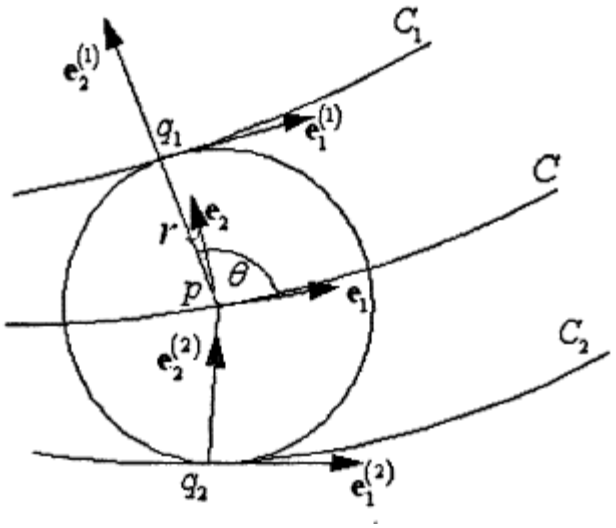

Fig. 3.3 The Frenet frames of medial and boundary curves

As can be seen from Figure 3.3, the boundary curve and the medial axis of the moving frame has the following mapping relationship:

$$\left.\begin{aligned} e_1^{(1)} &= e_1\sin(\theta) - e_2\cos(\theta) \quad (a) \\ e_2^{(1)} &= e_1\cos(\theta) + e_2\sin(\theta) \quad (b) \end{aligned}\right\} \quad (3.15)$$

$$\begin{aligned} e_1^{(2)} &= e_1\sin(\theta) + e_2\cos(\theta) \quad (a) \\ e_2^{(2)} &= -e_1\cos(\theta) + e_2\sin(\theta) \quad (b) \end{aligned} \quad (3.16)$$

Where θ is the angle of $\mathbf{q_1p}$ or $\mathbf{q_2p}$ and $\mathbf{e_1}$.

According to the principle of the accompanying curve in differential geometry, the two boundary curves and the medial axis can be regarded as two pairs of matching curves, respectively. Then the boundary curve can be expressed as follows:

$$\begin{aligned} r_1 &= r + re_2^{(1)} \\ r_2 &= r - re_2^{(2)} \end{aligned} \quad (3.17)$$

Where r is the radius of the medial transformation circle and $\mathbf{r}$ is the vector of point P on medial axis. $\mathbf{r_1}$ and $\mathbf{r_2}$ are the vector of q_1 and q_2 points on the boundary curve, respectively. From the

equation (3.15) - (3.17), we can see the relationship between the central axis and the boundary curve. In order to establish the relationship between the parameters of the medial axis and the boundary curves, the two sides of the equation (3.17) are differentiated at the same time, as follows:

$$\left.\begin{aligned} dr_1 &= dr + e_2^{(1)}dr + rde_2^{(1)} \\ dr_2 &= dr - e_2^{(2)}dr - rde_2^{(2)} \end{aligned}\right\} \quad (3.18)$$

Using the Frenet frame formula of the planar domain, equation (3.18) can be further simplified to:

$$\left.\begin{aligned} e_1^{(1)}\left(1+rk_1\right)ds_1 &= e_1 ds + e_2^{(1)}dr \quad (a) \\ e_1^{(2)}\left(1-rk_2\right)ds_2 &= e_1 ds - e_2^{(2)}dr \quad (b) \end{aligned}\right\} \quad (3.19)$$

Where k_1 and k_2 are the curvatures of the boundary curves C_1 and C_2 at point q_1 and q_2. By making dot product of $e_1^{(1)}$, $e_1^{(2)}$ to both sides of equation (3.19) (a) and (b), we could get as follows:

$$\left.\begin{aligned} \frac{ds_1}{ds} &= \frac{\sin(\theta)}{1+rk_1} \\ \frac{ds_2}{ds} &= \frac{\sin(\theta)}{1-rk_2} \end{aligned}\right\} \quad (3.20)$$

From equation (3.20) can be obtained between the natural parameters of the medial axis and the boundary curve, the scale relationship could be revealed. When we dot product $e_2^{(1)}$, $e_2^{(2)}$ at both ends of (a) and (b), we obtain the differential equation that r and θ should satisfy, which is equation (3.8).

Taking differential of equation (3.15), (a), (b) on both sides at the same time, we could get as follows:

$$\left.\begin{aligned} de_1^{(1)} &= \sin\theta de_1 + e_1\cos\theta d\theta - \cos\theta de_2 + e_2\sin\theta d\theta \\ de_1^{(2)} &= \sin\theta de_1 + e_1\cos\theta d\theta + \cos\theta de_2 - e_2\sin\theta d\theta \end{aligned}\right\} \quad (3.21)$$

Using the Frenet frame formula of the planar domain, equation (3.21) can be further reduced to:

$$\left.\begin{aligned} k_1 ds_1 &= kds + d\theta \\ k_2 ds_2 &= kds - d\theta \end{aligned}\right\} \quad (3.22)$$

By substituting equation (3.20) into equation (3.22), we can get the relationship between the curvature k of the medial axis at the point P and the curvature k_1, k_2 of the boundary curve at the corresponding tangent points, which is equation (3.14).

From the equations (3.13) and (3.14), we can see that when $(1 + k_1 r)(1 - k_2 r) = 0$, the two equations are meaningless; when the radius of the medial transformation circle is equal to the radius of curvature a point on the boundary curve, it equals to an endpoint on the central axis. Thus, this condition can be used as an end condition for the following recursive algorithm.

3.1.3 Tracing algorithm of medial axis transformation

In order to construct the tracking algorithm for solving the medial axis, we can obtain the coordinates of the point P on medial axis and the corresponding tangent point q1 and q2 by iteration or other methods. Then, $e_2 = q_1q_2 / \|q_1q_2\|_2$, e_1 is perpendicular to e_2, and follows the right hand system, e_3 perpendicular to the paper outwards. $\theta = \arccos(q_1p \cdot e_1 / r)$, the curvature of the medial axis at point P can be calculated by equation (3.14). According to the

Taylor expansion formula and the Frenet formula of the planar domain, if the third order small number is omitted, the vector equation of the next point p* adjacent to point P is:

$$r_{\rho^*} = r(s) + \Delta s e_1 + \frac{1}{2} k \Delta s^2 e_2 \quad (3.23)$$

Where s is the central axis at point P along the e_1 direction of the arc derivative. Figure 3.4 shows that the Frenet frame at point p* can be written as:

$$\left.\begin{aligned} e_1^* &= e_1 \cos\delta + e_2 \sin\delta \\ e_2^* &= -e_1 \sin\delta + e_2 \cos\delta \end{aligned}\right\} \quad (3.24)$$

Where $\delta = \Delta s/\rho$, $\rho = 1/k$ is the radius of curvature circle at point P on the medial axis.

According to equation (3.11) or equation (3.20), we can get the parameters ΔU_1, ΔU_2, or ΔS_1, ΔS_2 in the curves C_1 and C_2, and then we can get corresponding parameters for all the points under the boundary curve:

$$\left.\begin{aligned} u_1^* &= u_1 + \Delta u_1 \\ u_2^* &= u_2 + \Delta u_2 \end{aligned}\right\} \quad (3.25)$$

Substituting parameters of u_1^*, u_2^* into the curve C_1, C_2 equation, you can get the tangent points corresponding with p* points, q_1^* and q_2^*. Using the curvature equation (3.26), we can obtain the new parameters and corresponding curvature on the boundary curve, as follows:

$$k_i^* = \frac{\left\| \dot{r}_i \times \ddot{r}_i \right\|_2}{\left\| \dot{r}_i \right\|_2} \quad i = 1, 2 \quad (3.26)$$

Thus, we can get the curvature of the next point p* to obtain the next point p* on the medial axis, and the coordinates of the new tangent points q_1^* and q_2^* corresponding to p* and the new Frenet

frame. Followed by repeated recursion, the medial axis and medial transformation circle could be achieved.

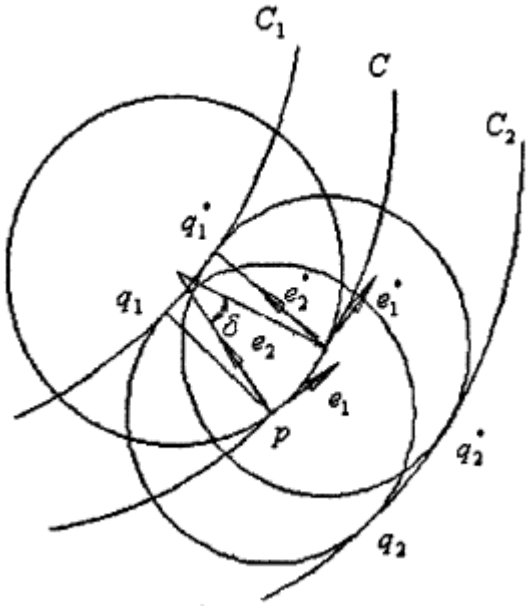

Fig. 3.4 Tracking algorithm of the medial axis

3.2 Bifurcation and Endpoint Processing

As mentioned earlier, for the connection field in the Euclidean plane the medial axis also includes the normal point, the bifurcation point, and the end point, and the calculation of the bifurcation point is the bottleneck of the precise calculation of the medial axis. Choi et al. have used the idea of regional decomposition to decompose complex regions into simple regions that do not contain bifurcation points, which avoids dealing with bifurcation points; however, the specific operations are complicated and need to be iterated again to limit the idea to be widely used [3].

In this paper, the bifurcation point is determined by the following method. According to the previous axis tracking algorithm to determine the next point on the medial axis, we need to calculate the distance from point P to points on the curve. If the distance is greater than or equal to the radius of the center circle, it means that no bifurcation point has been encountered and the previous tracking algorithm continues to be executed. Otherwise, if the bifurcation point is encountered, the current P point and the corresponding tangent point could be recorded. In the calculation of distance, to speed up the iterative process, the tracked parts do not need calculation. Ramanathan et al. suggested that if the two boundary curves have a common vertex, when the medial axis transformation is made from the bifurcation point, the process does not need to judge the distance because there will be no bifurcation points [4].

As shown in Figure 3.2, the point q_3 is a new tangent point, where the point P is the bifurcation point. If we use q_3 to replace the original q_2 point, and the corresponding frame and curve parameters are updated, then we continue the previous tracking algorithm, C_{21}, which is the medial axis in this branch, so that it could be obtained. In this way, making q_3 instead the original q_1, we can find another branch of medial axis, which is C_{23}. If there are multiple tangent points at a time, the processing method is similar.

Another special point is the endpoint, where the medial transformation circle has only one tangent point with the boundary curve. The circle is also the curvature circle of tangent point, as shown in Figure 3.2, point p_1. For this kind of point, equations (3.13 and 3.14) fail, which can be used as an end condition of the tracking algorithm. The same kind of point can also be used as the starting point of the algorithm, and we can take derivative of curvature for the boundary

curve. When the derivative value is zero and the curvature value is positive, the extremum of the curvature is the endpoint. At this time, the two tangent points coincide. For the two equations to be valid, the radius r of the center circle should be increased by an infinitely small ε.

Thus, we have a solution to deal with a variety of points on the medial axis and the tracking algorithm pseudo-code is as follows:

Tracing Algorithm (Given (p, q_1, q_2, Δs))

Do {

Calculate the unit vector e_1 and e_2: $e_2 = q_1q_2 \,/\, \|q_1q_2\|_2$ $e_1 \perp e_2$

The radius of medial transform circle r: $r = \|p - q_1\|_2$

The angel θ between q_1p or q_2p and e_1: $\theta = \arccos(q_1p \cdot e_1 \,/\, r)$

Calculate the curvature k at the point P of the medial axis and the moving instantaneous line using equation (3.14)

Use equation (3.23) to calculate the coordinates of the next point p*;

Update the corresponding Frenet frame according to equation (3.24);

The parameter increment of the boundary curve is obtained by the equation (3.11) or (3.20), as ΔU_1, ΔU_2 or ΔS_1, ΔS_2

$\Delta u_1 = \Delta s_1 \,/\, \|r_1\|_2$

$\Delta u_2 = \Delta s_2 \,/\, \|r_2\|_2$

The coordinates of the tangent points, q_1^* , q_2^* are updated according to the known curve parameter equation;

Using equation (3.26), we can calculate the new tangent points, q_1^* , q_2^*, and corresponding curvatures k_1 and k_2 on the boundary curve to calculate the distance $|pq_2|$, and to calculate the minimum distance d_{min}, and judge whether it is less than r;

If ($d_{min} < r$), record p, q_3, and q_2;

$p = p^*$, $q_1 = q_1^*$, $q_2 = q_2^*$;

}

While ($1 + rk_1 ! = 0$ & $1 – rk_2 ! = 0$)

Now have p, q_3, and q_2; Repeat the above tracking algorithm to calculate the rest branch;

END

3.3 The Exact Solution for Medial Axis Transformation

3.3.1 Two tangent points circle exact solution

The above tracking algorithm can be used to calculate the medial axis of the boundary curve on planar domain, but the accuracy of the tracking algorithm largely depends on the size of the arc length of the selected axis. If ΔS is too small, it affects the program running time; on the other hand, if ΔS is too large, the calculation accuracy cannot guarantee to meet the needs of engineering applications.

In view of the above problem, this section uses a two tangent point circle algorithm, where only the case where the medial transformation circle and the boundary curves C_1 and C_2 are tangent to two points. In order to make the algorithm more efficient, we can refer to the result of the tracking algorithm discussed above as the initial condition of the two tangent point circle algorithm. The point P on medial axis, the boundary curves C_1 and C_2, and the corresponding

tangent points q_1 (u_1) and q_2 (u_2) are obtained by using the tracking algorithm. $\mathbf{e_1}$ and $\mathbf{e_2}$ are the unit tangent and the unit normal vectors of the medial axis MA at point P [5].

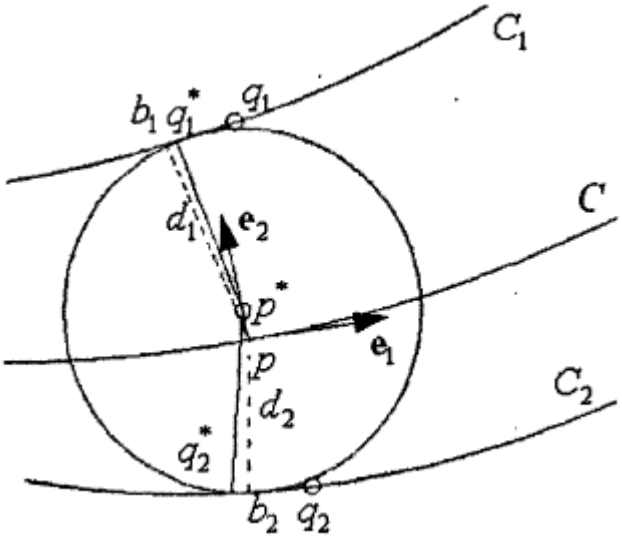

Fig. 3.5. Two tangent points circle algorithm

The minimum distance (d_1 and d_2) between point P and the boundary curves C_1 and C_2 can be calculated using the direct iterative method [6], given q_1 and q_2 as the initial values. If d_1 is greater than d_2, let point P go along the point e_2 direction to move a small step size Δ. Instead, let point p move a slight step in the opposite direction of e_2. Properly reduce the size of Δ until d_1 and d_2 are equal, which means the position of the center of the medial transform circle has been obtained. As shown in Figure 3.5, the pseudocode of this algorithm is given below:

Two Tangent Points Circle (p, u_1,u_2)

Calculate the unit vector e_1 and e_2;

Calculate the minimum distance d_1 and d_2 of the point p and the boundary curves C_1 and C_2

d_1 = Min Dis Between Point And Curve (p, u_1);

d_2 = Min Dis Between Point And Curve (p, u_2);

Do {

If ($d_1 < d_2$)

Do {

Cut stepdown: $\Delta = \Delta/2$;

Update p location: p = p-$\Delta * e_2$

New distance;

d_1 = Min Dis Between Point And Curve (p, u_1);

d_2 = Min Dis Between Point And Curve (p, u_2);

} while ($d_1 < d_2$)

Else {

Move to opposite direction, update p location: $\Delta = \Delta/2$; p = p+$\Delta * e_2$

Update distance:

d_1 = Min Dis Between Point And Curve (p, u_1);

d_2 = Min Dis Between Point And Curve (p, u_2);

}

}while ($|d_1 - d_2|$<distance tolerance)

END

3.3.2 Three tangent points exact solution

The so-called three tangent points circle algorithm, that is, the medial transformation circle and the boundary curve tangent to three points at the situation, uses the abovementioned process to determine the bifurcation point: in the tracking algorithm or two tangent points circle algorithm. The minimum distance between the current point and the boundary curve should be calculated

and checked whether it is less than the radius of the current medial transformation circle. If this distance is greater than the current radius, indicating that no bifurcation points have been encountered, the tracking algorithm and the two tangent points circle algorithm are continued. On the other hand, if the minimum distance is less than the current radius, this means current point P has passed the bifurcation point, and return to point P can get this bifurcation point. Based on the two tangent points circle algorithm, the pseudocode is as follows:

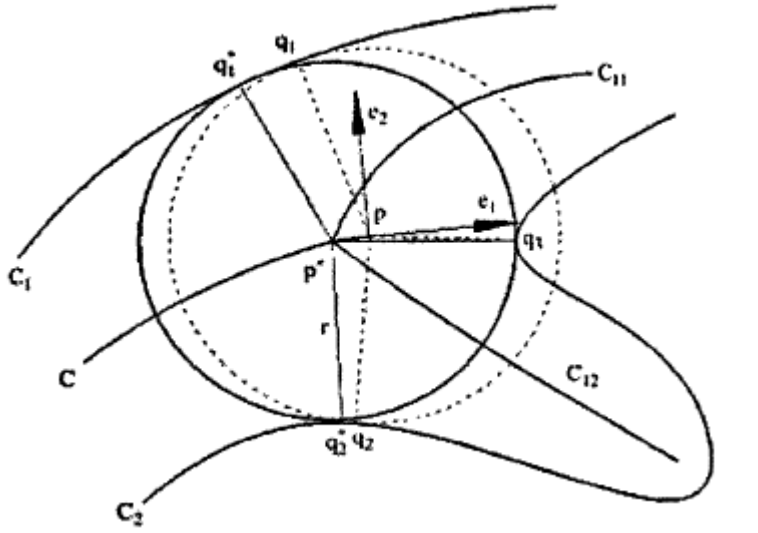

Fig. 3.6 Three tangent points circle algorithm

Three Tangent Points Circles (p, u_1, u_2, u_3)

Calculate the unit vector e_1 and e_2;

Calculate the minimum distance d_1 and d_3 of the point p and the boundary curves C_1 and C_2

d_1 = Min Dis Between Point And Curve (p, u_1);

d_3 = Min Dis Between Point And Curve (p, u_3);

Do {

If (d_1< d_3)

Do {

Cut stepdown: $\Delta = \Delta/2$;

Update p location: $p = p + \Delta * e_1$

New distance;

d_1 = Two Tangent Points Circle (p, u_1, u_2);

d_3 = Min Dis Between Point And Curve (p, u_3);

} while ($d_1 < d_3$)

Else {

Move to opposite direction, update p location: $\Delta = \Delta/2$; $p = p - \Delta * e_1$

Update distance:

d_1 = Two Tangent Points Circle (p, u_1, u_2);

d_3 = Min Dis Between Point And Curve (p, u_3);

}

}while ($|d_1 - d_3| >$ distance tolerance)

END

3.3.3 Overall Algorithm for Exact Medial Axis Transformation Solution

Now summarizing the above algorithms, they can merge into a coherent program. The first step is to find curvature extreme points of boundary curves, that is, the derivative value of curvature is zero and the curvature itself is positive; actually, it is the endpoint. As discussed above, this point can be used as a starting point for the program, and we store all of these endpoints in a starting endpoint table. Then, from an endpoint, we run the tracking algorithm and the two

tangent points circle algorithm until another endpoint appears. In this process, the minimum distance between the current point P on the medial axis and the discrete points of the boundary curve should be calculated. If the minimum distance is greater than the current radius of the medial transformation circle, this indicates the bifurcation point has not yet reached, and we continue to run the algorithm. If the minimum distance is less than the radius of current medial transformation circle, this indicates the bifurcation point has been encountered. In this case, the program is transferred to the three tangent points circle algorithm to get the bifurcation point p*. In addition, add point p*, q_3, and q_2 to the starting endpoint table, and use the new tangent point q_3 instead of the current tangent point q_2. Then, continue to track and the two tangent points circle algorithm; after each tracking cycle, the corresponding starting point must be removed from the table. The main program stops until all endpoints are run out, i.e., when the endpoint table is empty. Here is the pseudocode of the main program:

Begin Main Algorithm

Starting endpoints table (the derivative value of curvature is zero and the curvature itself is positive)

Do {

Tracking algorithm;

Two tangent points circle algorithm; \\ exact location of medial axis points

Calculate minimum distance between the current point p on the medial axis and the discrete points of the boundary curve, noted as d_{min}

If (d_{min} > r) continue algorithm;

Else {

Run three points circle algorithm to get medial axis point p* and tangent points q_1, q_2 and q_3;

Adding p*, q3, and q2 to starting endpoints table,

Using p*, q_3 and q_1 as the current initial end points;

Update unit vector e_1 and e_2;

}

}while (starting table is not empty)

END

3.4 The Equidistant Operation

Offsetting the curve as an important geometric operation in CAD/CAM system has direct application in tool path planning of CNC machining. It has also been applied in robot path planning, solid modeling, computer graphics, geomorphology, art pattern design, etc. We could not deny that the equidistant operation is a very difficult geometric operation, however, especially for nontraditional polygons and quadratic curves.

According to differential geometry concept of the equidistant line [6], we can see that for a given curve C: r (t) = (x (t), y (t)), with offsetting distance d, the equidistant line formula is:

$$r_d = r(t) + dn(t) = \left[x(t) - d\frac{y'(t)}{\sqrt{x'^2 + y'^2}} \right] i \pm \left[y(t) \mp d\frac{x'(t)}{\sqrt{x'^2 + y'^2}} \right] j \quad (3.27)$$

Where n(t) is the normal vector of the curve at a point, t is the parameter of the curve, and d is the distance to be offset.

The equidistant line may produce local or global self-intersection when the distance d (between the equidistant line and the original line) is large, or if the self-gap by detoured original line is less than 2d.

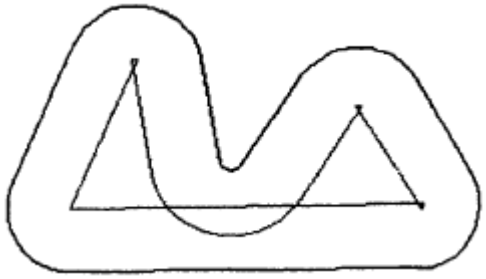

Fig. 3.7. Untrimmed offset curve

As shown in Figure 3.7, this phenomenon in the practical application of the equidistant line will result in serious consequences; dealing with these local or overall self-intersections one by one is very time-consuming. Choi et al. have given the mathematical theory of equidistant line of planar curve from the medial axis transformation perspective. The geometrical relationship between equidistant line and medial axis has been studied, and the equidistant line could be obtained via MAT [7]. He also classifies the points on the curve according to the local geometric properties and uses the regional decomposition. To ensure the continuity of the equidistant line, he introduced the concept of a single connected region to calculate the equidistant line. This method is simple but the process is relatively complicated. The author here suggested that, after running the tracking algorithm to obtain the medial axis, we could have the union of medial transformation circle of every boundary curve point. Is it possible to reverse the operation of the MAT to get the boundary curve, that is, the envelope line of medial transformation circles?

Let the medial axis equation be r(t)=(x(t), y(t)), where r is the radius of current medial transformation circle at point (x(t), y(t)). Then, we have the equation for medial transformation circles:

$$R = r(t) + re(\varphi) \quad (3.28)$$

And $e(\varphi) = \cos(\varphi)\dot{i} + \sin(\varphi)j$

Take derivatives on both side of (3.28) with t and φ

$$R = r(t) + re(\varphi) \quad (3.28)$$

$$R_i = x'i + y'j + r'e(\varphi) \quad (3.29)$$

Where $e_1(\varphi) = -\sin(\varphi)\dot{i} + \cos(\varphi)j$

Equations (3.19) and (3.20) are substituted into the following envelope conditions, i.e., the curve family has the same normal vector as the envelope line at the tangent point:

$$R_\phi = re_1(\varphi) \quad (3.30)$$

$$(k \times R_\phi) \square R_i = 0 \quad (3.31)$$

$$x'\cos\varphi + y'\sin\varphi + r' = 0 \quad (3.32)$$

$$\cos(\varphi - \alpha) = -r' / \sqrt{x'^2 + y'^2} \quad (3.33)$$

$$\varphi = \alpha + \pi \pm \arccos\left(r' / \sqrt{x'^2 + y'^2}\right) \quad (3.34)$$

Then substituting equation (3.34) into equation (3.28), we find:

$$R = r(t) + r\left[\left(\frac{-x'r' \pm y'\sqrt{x'^2 + y'^2 - r'^2}}{x'^2 + y'^2}\right)i + \left(\frac{-y'r' \mp y'\sqrt{x'^2 + y'^2 - r'^2}}{x'^2 + y'^2}\right)j\right] \quad (3.35)$$

If the arc length s is used as parameter and the formula (3.8) is taken into account, the equation (3.35) can be reduced to:

$$R = r(s) + re(\alpha \pm \theta) \quad (3.36)$$

Where, $e(\alpha \pm \theta) = \cos(\alpha + \theta)i + \sin(\alpha + \theta)j$ is the normal vector of the boundary curve at the tangent point. α is the angel between e_1 and i. It can be seen from the equation that the tangent point of the medial transformation circle and the boundary line is exactly the element of the envelope curve, and these points are called feature points in the differential geometry [8].

According to the envelope conditions, we can see that at this point, the medial transformation circle and the boundary curve have a common normal vector, so that the equation of the boundary curve can be introduced as follows:

$$R_d = r(s) + (r - d)e(\alpha \pm \theta) \quad (3.37)$$

Here, d is the offsetting distance, if $(r - d) < 0$, we could let $r = d$ to avoid self-intersection.

Reference

[1] Ding, Donghong, Zengxi Pan, Dominic Cuiuri, and Huijun Li. "A practical path planning methodology for wire and arc additive manufacturing of thin-walled structures." Robotics and Computer-Integrated Manufacturing 34 (2015): 8-19. doi:10.1016/j.rcim.2015.01.003.

[2] Cao, Lixin, and Jian Liu. "Computation of medial axis and offset curves of curved boundaries in planar domain." Computer-Aided Design 40, no. 4 (2008): 465-75. doi:10.1016/j.cad.2008.01.002.

[3] Choi, Hyeong In, Sung Woo Choi, Hwan Pyo Moon, and Nam-Sook Wee. "New Algorithm for Medial Axis Transform of Plane Domain." Graphical Models and Image Processing 59, no. 6 (1997): 463-83. doi:10.1006/gmip.1997.0444.

[4] Ramanathan, M., and B. Gurumoorthy. "Constructing medial axis transform of planar domains with curved boundaries." Computer-Aided Design 35, no. 7 (2003): 619-32. doi:10.1016/s0010-4485(02)00085-4.

[5] Choi, Hyeong In, Sung Woo Choi, Chang Yong Han, Tae-Wan Kim, Song-Hwa Kwon, Hwan Pyo Moon, Kyeong Hah Roh, and Nam-Sook Wee. "Two-dimensional offsets and medial axis transform." Advances in Computational Mathematics 28, no. 2 (2007): 171-99. doi:10.1007/s10444-007-9036-5.

[6] Kühnel, Wolfgang, and Bruce Hunt. Differential geometry: curves, surfaces, manifolds. Providence, RI: American Mathematical Society, 2015.

[7] Cao, Lixin, and Jian Liu. "Computation of medial axis and offset curves of curved boundaries in planar domain." Computer-Aided Design 40, no. 4 (2008): 465-75. doi:10.1016/j.cad.2008.01.002.

CHAPTER 4:

Title: A Medial Axis Transformation based Process Planning Method for Rapid Laminated Tooling

Author: Ziyang He[1], Matthew Frank[1, *]

1. Department of Industrial and Manufacturing System Engineering, Iowa State University, Ames, IA 50011, United States

Corresponding author: heziyang@iastate.edu

Abstract:

This paper presents an algorithm to automatically select the positions for friction stir spot welding (FSSW) in a laminated rapid tooling process. The work combines a two-dimensional structural analysis with tool path planning to realize the overall process planning for the rapid tooling of a plastic injection mold. The work starts from a two-dimensional cantilever beam model, defining the effective distance of a single spot joint strength, and also considers the effect of a single layer thickness. Secondly, an efficient medial axis transformation algorithm, which is suitable for the general two-dimensional boundary curves, has been proposed to generate the adaptive equidistance offsetting curves. In addition, through different working conditions of the internal and external spot welds, an adaptive discretization method is presented. Then, a selection principle for choosing the initial spot weld location and processing order with optimization to avoid redundancy is presented. Finally, the authors compare the advantages of this novel

algorithm and traditional path planning algorithms with respect to strength and processing efficiency while taking into account structural strength.

Keywords: Friction Stir Spot Welding, Rapid Tooling, Structural Modeling, Medial Axis Transformation, Process Planning

1. Introduction

Nowadays, with rapid development of additive manufacturing, rapid tooling processes have stepped into the vision of both researchers and industrial users [1]. Laminated rapid tooling belongs to the laminated object manufacturing (LOM) conceptual framework. Previous studies are heavily based on non-metallic materials, such as paper and plastics, and layers are bonded with adhesives [2]. There are several attempts to combine laser based welding technique into rapid tooling system [3]. But the there are two severe pending problems, one is lacking of strength for non-metallic materials. Usually, users are just using non-metallic mold as the female mold or just showing the conceptual design [4]. The other problem is large heat influx during the laser based welding process, like cycling heat treatment process, which will cause inaccurate geometry presentation and micro-structural problem (e.g. internal voids and large dendrites formation) [5].

The Rapid Prototyping and Rapid Manufacturing Lab in Iowa State University, has proposed and introduced a new hybrid additive/subtractive rapid tooling system [6]. This new system has combined friction stir welding and post CNC machine seamlessly, which has brought the hybrid

rapid tooling system into a different direction. In the proposed process, aluminum plates are first pressed onto a stack with glue and bonded. Both the adhesive and toe clamps serve as a combined temporary "clamp" to hold the plates together for spot welding. After gluing, the first step is to weld the boundary sacrificial wall, then proceed to weld down the interior cross-sectional loops of material for each layer (as shown in Fig. 1) [6]. Since this system could utilize existing CNC machines, existing tooling planning software and operation system, so it is promising to become an alternative solution to replace the laser welding based rapid tooling. For industrial application process, the automated process planning for this rapid tooling method is still uninvestigated. In this paper, a fully automatic process planning algorithm to take structural analysis into consideration will be developed.

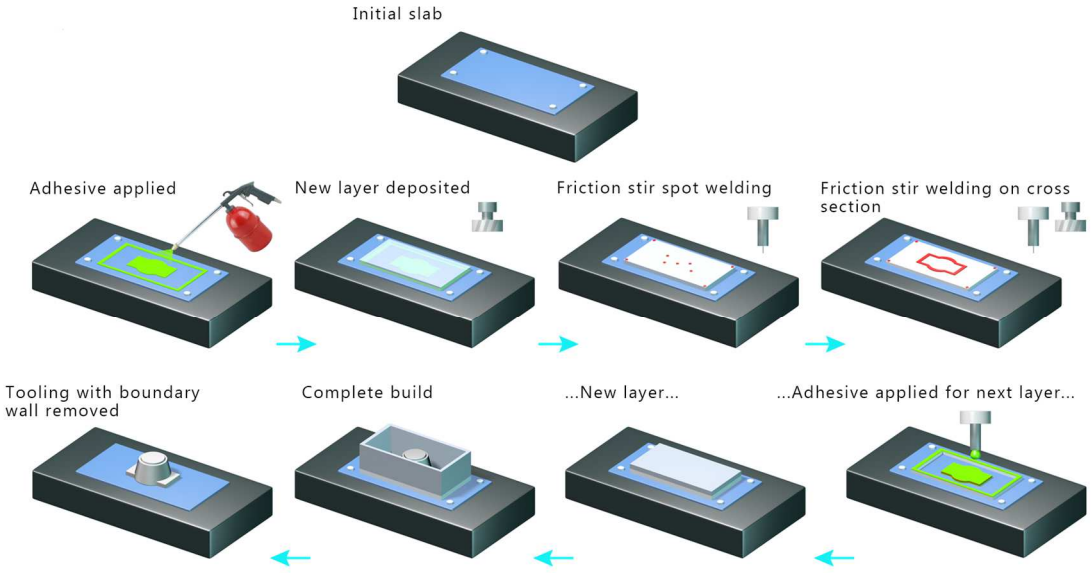

Figure 1. Schematic diagram of friction stir welding based manufacturing system [6]

For mainstream process planning or tool path planning methods in additive manufacturing area, there are several typical examples. Karunakaran et al. [7] used CNC machining to face mill each layer built by metal inert gas welding to significantly improve the dimensional accuracy of parts. Xiong et al. [8] incorporated a plasma torch into a traditional machine tool, realizing plasma welding and CNC finish machining on the same platform. Neither of them has considered strength and geometry requirements together. In nature of rapid manufacturing, specifically in the process planning stage, the mode of separating consideration of geometry and structural strength is not favorable. Some investigators have used modular analysis and finite element analysis (FEA) to evaluate the strength performance of additive manufactured parts, but these analysis are for post-manufacturing and global analysis. The layer based and pre-manufacturing (process planning stage) analysis, to author's knowledge, which could consider geometry and strength requirements simultaneously, has not been reported yet.

Medial axis transformation as a kind of pure geometry algorithm has been proposed by Blum et al. 1967, to estimate the minimum thickness of a planar domain [9]. It is well established to extract skeletons from 2D and 3D geometry which approximates the shape with a set of tangent spheres, and has already been applied into tool selection in high speed machining process. Unfortunately, the approximation algorithm and large computational load have become the biggest obstacles for its further application.

Hereon, this paper is intended to improve the traditional process planning method with an efficient medial axis transformation algorithm. A novel decomposition strategy which could

largely reduce computation load with enough accuracy has been introduced firstly. Additionally, considering the cantilever beam model as parameters of step over distance, a fully automated friction stir spot welding process planning algorithm has been developed and verified.

2. Methodology

As illustrated in Figure 2, this paper will present a method to determine spot weld locations of two metal plates in the aforementioned layer based tooling approach. The method involves selecting spot welds for both the outer wall and interior slice chains (Figure 2a). Whereas the outer walls are sacrificial, the previous alternating spot welding approach is used. In this manner, spot weld alternate from corners to wall midpoints. This paper, however, further addresses, the spot welds in the tooling cross sections which are further broken into boundary points, medial axis points and interior points (Figure 2b). The work of this paper will address individually, the generation of and selection of points along these boundaries culminating in a final section of required spot welds, as envisioned in Figure 2c. The following section, will begin with a structural model of the critical points along the slice boundaries.

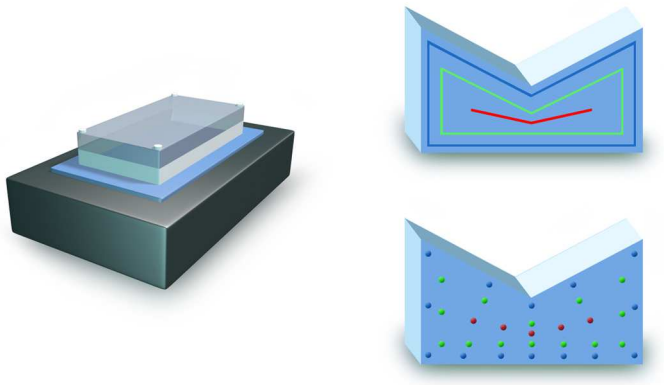

Figure 2. Friction Stir Spot Welding points definition and selections

2.1 Structural modeling

Hereon, we are considering to use a simplified cantilever beam with single free end to describe the physical conditions for this process, as shown in Fig. 3. We have also classified acting forces into three stages, manufacturing stage I (FSSW), II (CNC Machining) and working stage (Injection and de-molding).

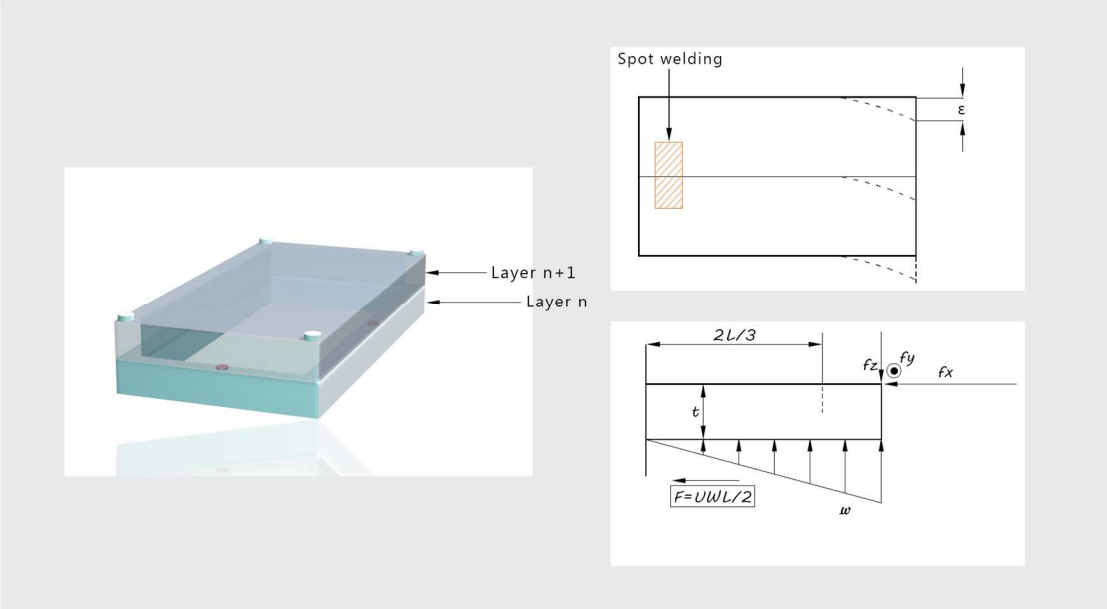

Figure 3. Structural modelling and effective distance

For manufacturing stage I, the shear force and pressure forces are two main factors in this stage. For rapid tooling process, the estimated shear force could reach 3 KN for a single FSSW spot. Since the shear forces could cause serious damages on tooling structure. We have defined an "in-plate" fixture technique to overcome the shear force during the first several spots, as shown in the Fig.3 (a). Additionally, this self-fixturing structure could also resist the overall part distortion

induced by heat influx and enhance the general stiffness during the manufacturing stage (I and II). And it could be removed when the mold core islands are finished, as the support structures. In order to avoid overlap the spot welding heat affect zone, we use a four side recentagular box outside those mold core islands as the boundary walls. There will be four spot welds in each layer which will be either in the corners of the boundary wall or in the mid span of the boundary walls. The location of the spot welds is alternated for subsequent layers as in Fig. 3 (a).

If the shear forces could be mainly resisted by the self-fixturing structure both in stage I and II, then as an additive/subtractive process, the as-received structure must survive after the machining process, that is, to resist the cutting force. The cutting forces are depended on main factors, such as materials properties, tool parameters and feed speed. Here, we use the following formulas to estimate cutting force in our rapid tooling system, with a range from several to tens newton. As shown in the Fig. 3 (b), the cutting forces and other arbitrary acting forces are normally decomposed into three directions, X axis (compress force), Y axis (bending force), Z axis (shear force). X axis and Z axis will be decided to meet the minimum number of spot welding sets. Y axis forces will be used to analysis a new concept, which we have firstly introduced here, “the safety affected zone”. We are using this zone to decide the maximum distance of two neighboring spots. As our optimization goal is trying to get less spots but enough structure stiffness to resist forces from both manufacturing and working conditions. Here, we have used a ramped bulking force distribution to stimulate the worst case scenario comparing to actual physical situation. Notably, as the friction existing between layers, the interlaminar friction forces should also be considered. So we have the following equations based on materials mechanics:

$$M = \frac{\mu w L t}{4} \quad (1) \qquad \delta = \frac{1}{EI}\left(\frac{FL^3}{3} - \frac{11wL^4}{120} - \frac{4M}{9} \cdot L^2\right) \quad (2)$$

By given the maximum deflection δ, we could easily get the effective distance, which is the largest safe distance for two adjunct spot welds. The t here, is the layer thickness. To be simplified, a "lumped" frictional force is assumed to act at x = 2L/3, which is the centroid for the ramped bulking normal force.

For the plastic injection molding process, we need to consider the bulking force caused by injection and demolding process. The injection force could be regarded as another kind of bending forces acting on the cantilever beam. But the demolding is usually larger than cutting force in a certain level, and could be estimated by using following equations:

$$F_e = \frac{\alpha(T_m - T_e) * E * A * \mu}{\frac{D}{2t} - \frac{D * \gamma}{4t}}$$

Where:

F_e = Ejection Force

α = coefficient of thermal expansion of moulding material

T_m= melting temperature of moulding material

T_e = ejection temperature of moulding material

D = diameter of core

E = Young's Modulus of moulding material at T_e

A = Area of contact between core and molding in direction of ejection

μ = coefficient of friction between molding material and core

t = thickness of molding

γ = Poisson's ratio for molding material

2.2 Medial Axis Transformation

Medial Axis Transformation, or skeletonization, has been widely studied over the past few decades in the computer vision field. Lee [10] proposed a divide-and-conquer approach that constructs the generalized Voronoi diagram for simple polygons. The medial axis transformation can be easily extracted by removing the Voronoi edges connecting to concave vertices of the polygon. Srinivasan et al. [11] extends Lee's algorithm to computing a generalized Voronoi diagram for polygons with holes. Choi [12] presents an MAT approximation algorithm in the planar domain via domain decomposition. Kao [13] proposes a method that directly associates boundary points to the corresponding proximity metrics based on Lee's and Srinivisan's methodology. For "three-tangent-points-circle" and "two-tangent-points-circle" definition and algorithm and details of computation method are discussed in the chapter 3.

Figure 4. Medial Axis Transformation concepts and application in tool path planning

3. Development of overall algorithm towards automated process planning

For the overall algorithm process planning, it could be divided into several functional parts. For this paper, we are mainly discussing about adaptive medial axis transformation and its offsetting and discretization. After displaying the general algorithm (as shown in Fig. 5), two specific algorithm diagrams are picked up to show our design guidelines.

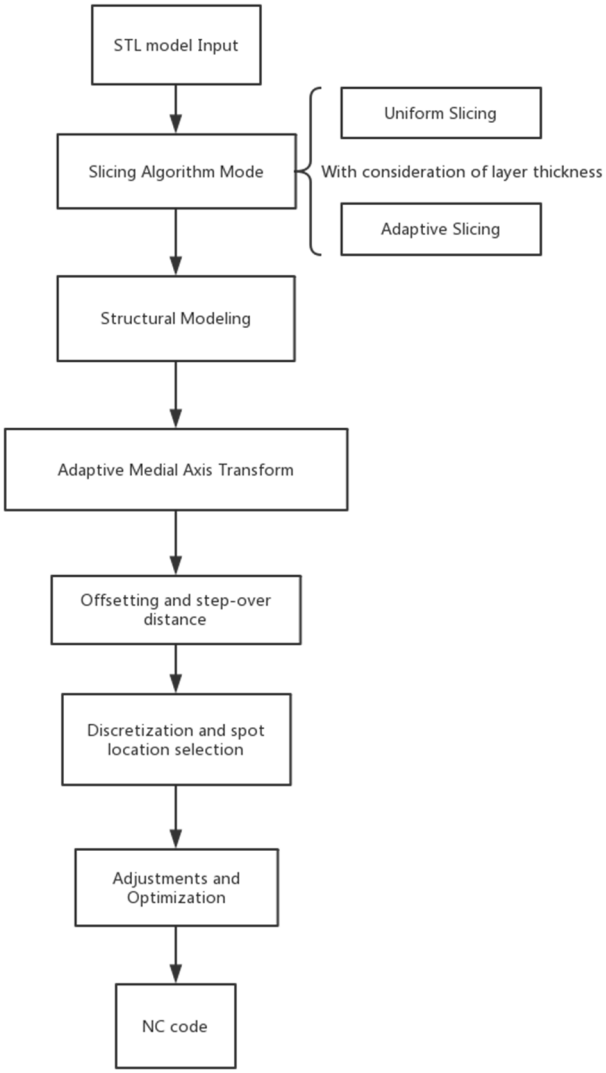

Figure. 5 General algorithm development and diagram

3.1 Adaptive domain decomposition and offsetting

Here, we only consider the cross section without holes, which is easily to be decomposed into several simple polygon domains.

We call the lines between three-tangent-point circle center and endpoint, the sub-skeleton lines. Then, we also define the lines between three-tangent-point circle center and two-tangent-point circle center, the skeleton lines type I. Lastly, the lines between two-tangent-points centers, are called the skeleton lines type II. The outside boundary curves are divided by those tangent points into boundary lines.

For the next step, we could connect three-tangent-points with end points, and connect tangent points with their centers, in order to divide the overall domains into different parts. The following diagram is acting as the classification method to sort these different areas into 3 types.

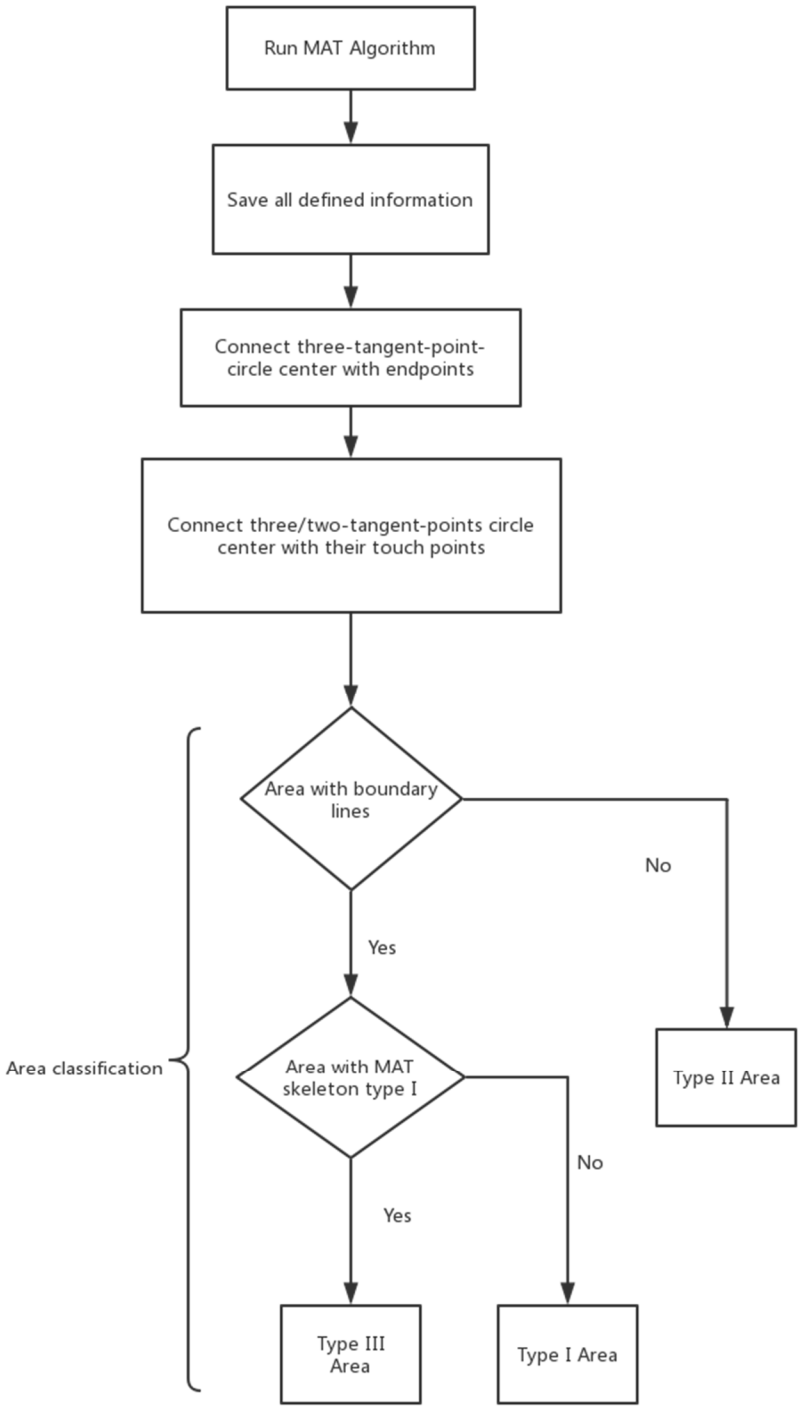

Figure. 6. Decomposition definition and strategy

The offsetting strategy is based on area classification. For type I area (triangle ABb0), we could parallel offset the boundary lines. For the type II area (triangle T2b1b2), we could parallel offset the type II skeleton lines. For the type III area (trapezoid BCb1b0), the offsetting is not parallel, since the nature that, the type Iii area is always sharing the boundaries with type I and II areas, so we could connect the intersection points to form the adaptive non-parallel offsetting. This adaptive method could solve big disadvantage of MAT-based offsetting from internal skeleton to outside, that is, it will generate discontinuity in order to cover the whole area, as shown in the Fig 7. Below.

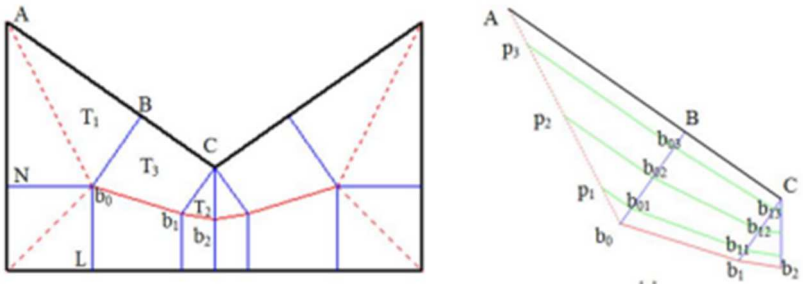

Figure 7. Offsetting example and points selection example

Additionally, due to the working conditions, we believe the outside points will bear more stress in plastic inject and demolding process, so we are using smaller effective distance to treat boundaries curves. For the internal points and points on the type I and II skeleton lines, we could use larger effective distance, in view of enhancing the processing efficiency. In this theory, any complex domain can be decomposed into these three fundamental shapes.

3.2 Discretization and spots point location selection

From 3.1, we have already developed a method to generate adaptive equidistance offsetting curves. These curves has provided potential union for selecting spots welding point location. But here, we are still lacking two criteria to discrete (disperse) the points and determine the adding/removing points for the gaps between boundary curves and skeletons (MAT).

For the first problem, we are here introducing a robust sampling algorithm, targeting at dispersing the achieved adaptive equidistant offsetting curves. There are three main methods for discrete sampling of plane curves: (1) Raster method, first rasterize the plane area where the curve is located, and then intersect the curve and grid lines as discrete sampling points. The resulting sampling points usually have a large amount of data, and the set of sampling points cannot reflect the local geometric characteristics of the curve well.

(2) Predictive projection method, that is, from the point of the curve, according to the curvature of the curve at that point, along the tangent direction of the point forward a short section to get the forecast point, and then projected to the curve to get the sampling point. Since the method includes a projection process, the computational complexity is large;

(3) ε -sampling method, the processing object is a plane closure curve, the sampling conditions are: set the curve point to the sampling point of the nearest distance d_1, to the plane of the curve area surrounded by the nearest distance d_2. If a sampling point set satisfies $d_1 < \varepsilon \times d_2$ at any point on the curve, it is the set of points, and ε is in the range $0 < \varepsilon < 1$. Since the method sets the parameter ε, it is necessary to find the appropriate ε value for the different graphs to satisfy the

sampling condition, so the set of sampling points is filled with uncertainty. In this paper, a sampling algorithm for simple plane closure curve is presented.

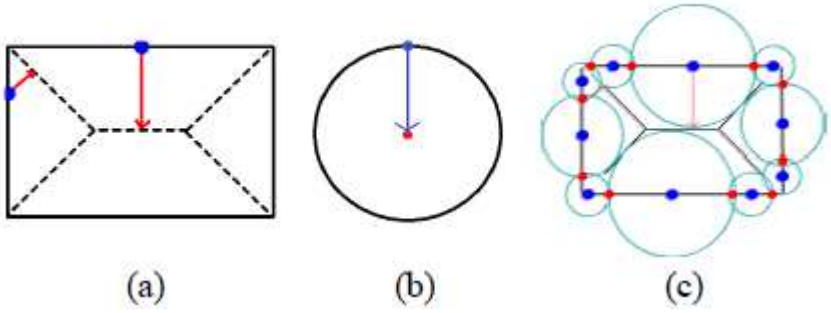

Figure. 8 Schematic example of dispersion sampling algorithm

The main steps of the sampling process:

(1) Calculate the medial axis of the planar domain and complete the offsetting process as prescribed in 3.1

(2) Pick up any point from the largest diagonal distance of boundary curve (offsetting curves) as the first point

(3) Evenly sampling the curve with “effective distance”, and calculate the local feature size of each point, so-called local feature size refers to the nearest distance to the axis, as shown in Figure 8 (a), (b), (c).

(4) If the distance is smaller than “effective distance”, the corresponding MAT point should be removed, means that the effect zone of boundary point is enough to cover the medial axis point.

(5) If the distance is larger than the effective distance, then put additional point at the middle point of distance (gap), then double check the new distance, to ensure the gap is smaller than effective distance

(6) Save all the points in a table, along with the slicing file as FSSW points

Because of large manufacturing force and working loading during plastic injection process, we have ranked boundary points as the first priority to maintain. The MAT points and interior points are acting as secondary supporting strengthen points.

4. Case study

A case study has been conducted to verify the stress distribution of both the proposed and zig-zag process planning method via FEA. The FEA approach considered individual layers and adhesive layers as solid elements, frictional interactions between laminations as contact elements, and a quadratic finite element mesh was applied. To make the result persuasive, an intensive three-dimensional level mesh has been adapted, which is close to the actual working and manufacturing conditions. For this study, we are using two AA6061 aluminum plate (150 mm *100mm*6mm), with tensile yield strength of 276 MPa and shear strength 207 MPa. The FSSW tool diameter is 6.0 mm, with rotation speed at 1400 RPM and plug-in speed at 20 mm/min. When the algorithm from section 3.2 was executed, the gap between MAT and boundary points is smaller than the effective distance, which is 48.3 mm based on aforementioned parameters. We intentionally ignored some boundary points, and only considered four endpoints on the corner to validate the efficiency of the proposed algorithm.

Then, stacked layers have been analyzed for horizontal and vertical stress distribution and deformation situations. It is notable that since the yield strength is the criteria for plastic deformation, and stress greater than the yield strength will result in irreversible deformation. We will consider this type of plastic deformation as a failure.

From Figure 9, we could easily see that even with fewer boundary points, the proposed structure has shown a strong resistance to vertical loading. Since vertical loading is mainly from the demolding process, any failure during this process would be a major concern. Admittedly, without defined support from boundary points, the shear stress from manufacturing stage would be difficult to resist, and that is also the reason we are using the boundary wall structure as the self-fixturing structure during the FSSW processing. Notably, even if the shear force from one horizontal side is large, shear forces of less than 207 MPa for this study implies no plastic deformation occurs during the process.

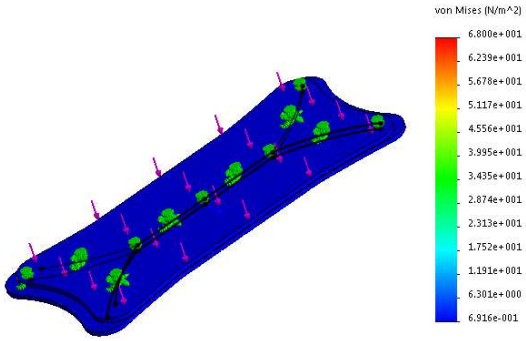

(a) Vertical load stress distribution

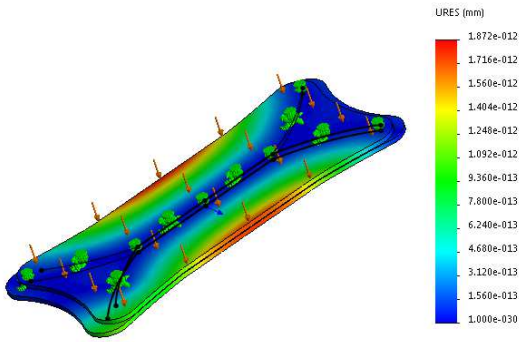

(b) Vertical load deformation

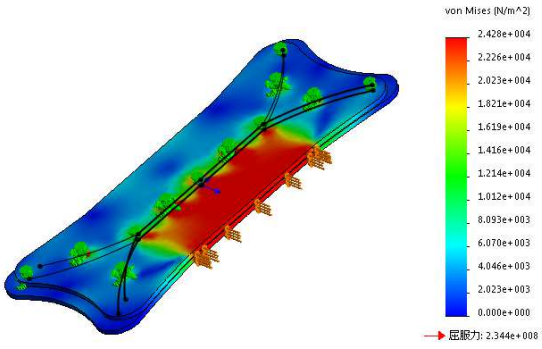

(c) Horizontal load stress distribution

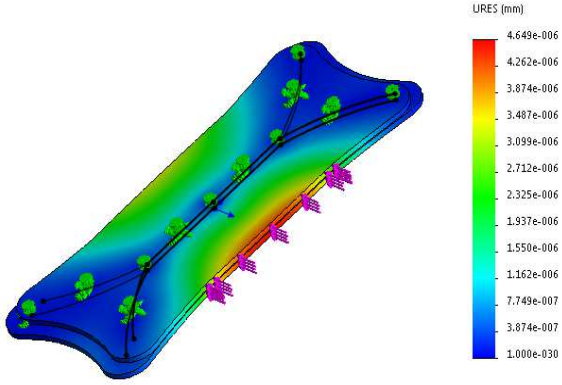

(d) Horizontal load deformation

Figure. 9 Deformation and stress distribution for MAT based process planning

To make the result persuasive, a comparison of the traditional algorithms based on a zig-zag method is also presented. The method is based on a grid layout of many points distributed across the board, with the effective zone overlapped. This method is a traditional spot welding

patterning method with various applications. From Figure. 10, due to more heat influx and large plug-in forces, we could notice that there were some areas with plastic deformation at the corners. When the horizontal load was applied, the plastic deformation region appeared at boundary curves near corners. We believe this phenomenon is due to the overlap of both the heat affected zone and mechanics effective zone, which leads to the conclusion that a larger number of spot welds is not better; it could even cause some failures on the boundary and corners.

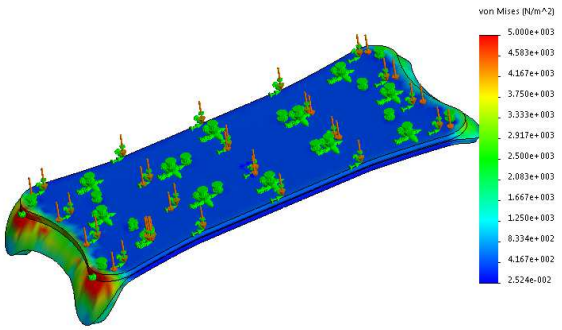

(a) Vertical load stress distribution

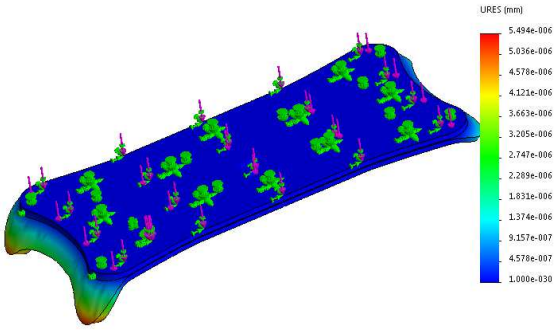

(b) Vertical load deformation

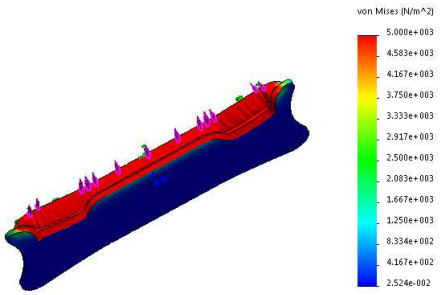

(c) Horizontal load stress distribution

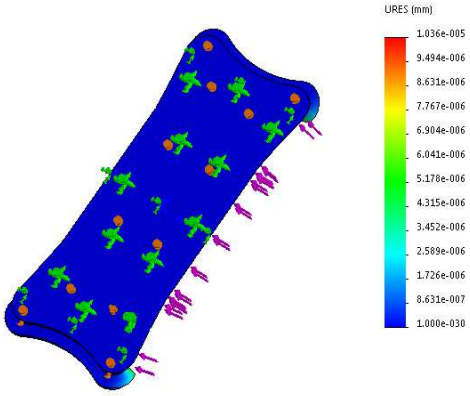

(d) Horizontal load deformation

Figure. 10 Deformation and stress distribution for Zig-zag based process planning

Methods		Zig-zag Method	MAT Method
FSSW Spots	First	12	7
	Second	12	6
Shear stress (MPa)		8.6	8.9
Tensile stress (MPa)		17.2	16.3
Deflection(mm)		0.29	0.21

Table 1. Parameter and performance comparison between two methods

From the comparison, regardless of the fact that minor plastic deformation occurred, the MAT method with a lower number of FSSW spots can better satisfy the strength requirements compared to the zig-zag method. Using 50% less spot welds shows that the MAT method is far more efficient and should be more cost effective.

5. Conclusion

In this paper, a fully automated process planning method with consideration of component strength requirement has been developed. Although the way to integrate strength and structural model is still in the preliminary stage, it shows the future direction, to consider the strength requirement locally and in the pre-manufacturing stage process. Additionally, by using medial axis transformation, a pure geometric method, we have successfully analyzed strength requirement layer by layer without using finite element analysis (FEA). Last but not least, the case studying has shown, even without much less spot number, the testing tensile strength is only 13.7% less than previous continuous Friction Spot Welding (FSW) rapid manufacturing method and 9.7% less than Zig-Zag traditional planning method. Notably, the stress distribution has been

optimized to a much better level comparing to previous two methods. The future works could be done in following areas: 1) What is the optimal sequence of these selected spots due to the large heat influx of Friction Stir Spot Welding (FSSW); 2) How could we combine light weight post manufacturing stress analysis (like modular analysis) solver with this pre-manufacturing algorithm, to provide some basic design guidelines? Because this could additionally put the computational load and reduce the process planning time.

Reference

[1] Wimpenny, D.i., B. Bryden, and I.r. Pashby. "Rapid laminated tooling." Journal of Materials Processing Technology 138, no. 1-3 (2003): 214-18. doi:10.1016/s0924-0136(03)00074-8.

[2] Chiu, Y.y., Y.s. Liao, and C.c. Hou. "Automatic fabrication for bridged laminated object manufacturing (LOM) process." Journal of Materials Processing Technology 140, no. 1-3 (2003): 179-84. doi:10.1016/s0924-0136(03)00710-6.

[3] Akula, Sreenathbabu, and K.p. Karunakaran. "Hybrid adaptive layer manufacturing: An Intelligent art of direct metal rapid tooling process." Robotics and Computer-Integrated Manufacturing 22, no. 2 (2006): 113-23. doi:10.1016/j.rcim.2005.02.006.

[4] Bassoli, Elena, Andrea Gatto, Luca Iuliano, and Maria Grazia Violante. "3D printing technique applied to rapid casting." Rapid Prototyping Journal 13, no. 3 (2007): 148-55. doi:10.1108/13552540710750898.

[5] Ding, Donghong, Zengxi Pan, Dominic Cuiuri, and Huijun Li. "A practical path planning methodology for wire and arc additive manufacturing of thin-walled structures." Robotics and Computer-Integrated Manufacturing 34 (2015): 8-19. doi:10.1016/j.rcim.2015.01.003.

[6] Abdelall, E.S., Frank,M.C, and Rivero,I.V(2017). Rapid Tooling using Friction Stir Welding and Machining, Rapid Prototyping Journal ,23(1).

[7] Karunakaran, K.p., S. Suryakumar, Vishal Pushpa, and Sreenathbabu Akula. "Low cost integration of additive and subtractive processes for hybrid layered manufacturing." Robotics and Computer-Integrated Manufacturing 26, no. 5 (2010): 490-99. doi:10.1016/j.rcim.2010.03.008.

[8] Xiong, Xinhong, Zhang Haiou, and Wang Guilan. "A new method of direct metal prototyping: hybrid plasma deposition and milling." Rapid Prototyping Journal 14, no. 1 (2008): 53-56. doi:10.1108/13552540810841562.

[9] H. Blum, "A Transformation for Extracting New Descriptions of Shape," Models for the perception of speech and visual form, W. Wathen-Dunn (editor), MIT Press, pp362-380, 1967.

[10] D. Lee, "Medial axis transformation of a planar shape," Pattern Analysis and Machine Intelligence, IEEE Transactions on, pp. 363-369, 1982.

[11] V. Srinivasan and L. R. Nackman, "Voronoi diagram for multiply-connected polygonal domains 1: algorithm," IBM Journal of Research and Development, vol. 31, pp. 361-372, 1987.

[12] H. I. Choi, S. W. Choi, H. P. Moon, and N.-S. Wee, "New algorithm for medial axis transform of plane domain," Graphical Models and Image Processing, vol. 59, pp. 463-483, 1997.

[13] J.-H. Kao, "Process planning for additive/subtractive solid freeform fabrication using medial axis transform," Citeseer, 1999.

Appendix A: Medial Axis Transformation Code (MATLAB Version)

```
clear
clc
close all
\\ read picture file binary
% im=imread('input.jpg');
 [filename,pathname,filter] = uigetfile({'*.jpg;*.jpeg;*.bmp;*.gif;*.png'}, 'Selecting Pictures');
if filter == 0
   return
end
str = fullfile(pathname,filename);
I=imread(str);
im=I;
\\ Getting the dimensions
 [M,N,C]=size(im);
\\ Rotate grayscale
if C>1
   I_gray=rgb2gray(im);
else
   I_gray=im;
End
\\ Display
figure
```

```
imshow(im)
title(‘orginal picture’);
\\ Display
figure
imshow(I_gray)
title(‘Grayscale picture’);

\\ Binary Conversion
% I_bw=im2bw(I_gray,0.1);
I_bw=im2bw(I_gray);
I_bw=~I_bw;

\\ Display
figure
imshow(I_bw);
title(‘Binary Picture’);

\\ Binary Medial Axis Transformation
% I_bw=bwmorph(I_bw,'fill');
% PZ=bwareaopen(I_bw,5000);
% figure(4)
% imshow(PZ);
% title(‘Remove irrelevant elements picture’);
```

```
PZ=I_bw;
\\ Corrosion operation
SE=ones(20);
PZ=imerode(PZ,SE);
PZ=imerode(PZ,SE);
\\ Display
figure
imshow(PZ);
title(‘Medial Axis Transformation Picture’);
\\ Get the initial skeleton
PZ=bwmorph(PZ,'skel',250);
\\ Display
figure
imshow(PZ);
title(‘initial skeleton’);
PZ=bwmorph(PZ,'spur',5);
\\ Display
figure
imshow(PZ);
title(‘No spur’);
\\ Save final binary skeleton
imwrite(PZ, ‘Final skeleton’);
```

```
 [row,col]=find(PZ);
leg=length(row);
for i=1:leg
    im(row(i),col(i),1)=255;
    im(row(i),col(i),2)=0;
    im(row(i),col(i),3)=0;
end
figure
imshow(im);
title('Result on original picture');
```